1

Reactions of Aldehydes and Ketones and their Derivatives

S. R. Hussaini

Department of Chemistry and Biochemistry, The University of Tulsa, Tulsa, OK, United States

CHAPTER MENU

Organic Reaction Mechanisms 2017, First Edition. Edited by A. C. Knipe and M. G. Moloney.

Formation and Reactions of Acetals and Related Species

Novel nitrated [6,6,6]-tricyclic acetal or ketals are prepared by an intramolecular annulation of *o*-carbonyl allylbenzenes. The proposed mechanism involves olefinic nitration, bis-cyclization, and tautomerization, followed by another nitration. Further tautomerization and dehydration give the product. Non-cyclic products are obtained when the deoxygenated groups are at 4,5-position rather than 3,4-position on the benzaldehyde skeleton.[1]

During the synthesis of sacrolide A, attempted deprotection of (**1**) gave the desired product (**2**) along with an unexpected contaminant (**3**) in substantial amounts. Formation of (**3**) was speculated to be the result of *E*/*Z* isomerization of the conjugated double bond and subsequent cyclic hemiacetal formation followed by dehydration (Scheme 1).[2]

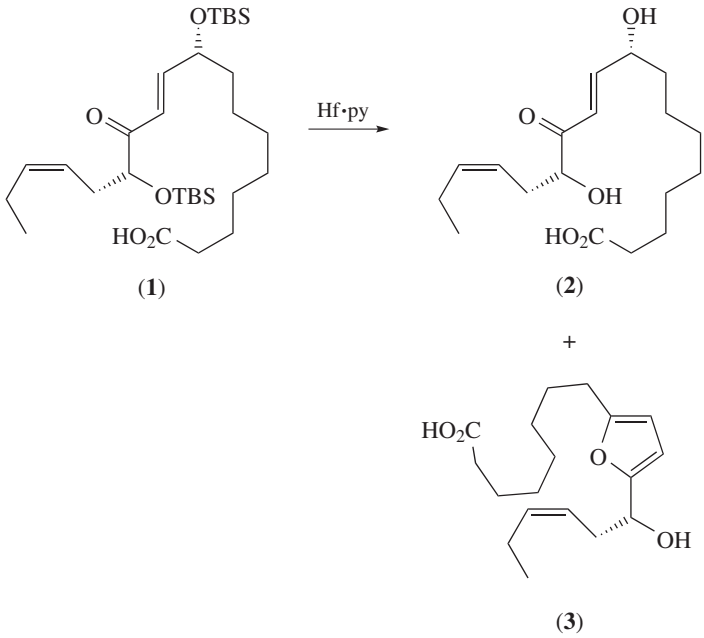

Scheme 1

Chloromethyl methyl sulfide/KI catalyses desilylation and acetal formation. The reaction also works with a combination of (ethylthio)methanol and TBDMSCl or TMSCl, but fails when only (ethylthio)methanol is used. On the basis of this information, and reactivity trends of aldehydes (electron-deficient aldehydes react faster), it is proposed that the active catalyst is methylene sulfonium halide (**4**), which activates the aldehyde and converts the OH group on the aldehyde into a better leaving group (Scheme 2).[3]

Acetal configuration interconversion is observed by ^{1}H NMR spectroscopy for the six-membered ring phenyl-substituted acetal during its formation from the corresponding diol. These diastereomers are hypothesized to interconvert as a result of acid catalysis under the reaction conditions.[4]

A gold(I)-catalysed ring opening of cyclic acetals and ketals by trimethylsilyl alkynes was achieved, which exploits the use of gold(I)-silicon catalysis. The reaction benefits from *in situ* and simultaneous generation of small amounts of a silicon-based super acid and a gold

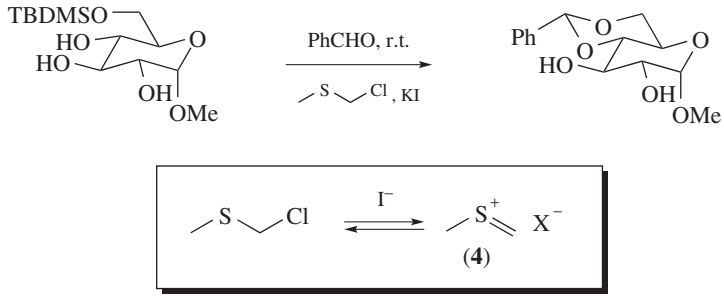

Scheme 2

alkynylide. The Lewis acid activates the electrophilic cyclic acetal or the ketal, while the *in situ* formed gold alkynylide, which is more nucleophilic than the parent alkynylsilane, attacks the acetal.[5]

Removal of the acetonide group from (**5**) does not result in the formation of expected product (**6**), and instead (**7**) is formed.[6] A plausible mechanism involves an acid-catalysed ring opening of acetonide via deprotonation. Finally, the acid-catalysed removal of hemiketal provides (**7**) (Scheme 3).

Substituted enaminoesters and acetal groups undergo an intramolecular cyclization with Lewis acids. The reaction probably undergoes a [1,5]-hydride shift after activation of the alkene by the Lewis acid. The zwitterionic intermediate undergoes the cyclization process, providing spirocycles. Density function theory calculations were performed to validate the proposed mechanism. Partial racemization observed in the process is explained using density functional theory (DFT) calculations.[7]

Reactions of Glucosides

Two isomeric glucosides hydrolyse at rates differing by 10^6-fold, despite the fact that they both give the same hydrolysed products (Scheme 4). Experimental and quantum chemical calculations revealed that ground-state destabilization and transition-state stabilizing effects are responsible for the observed reactivity differences. The ground-state destabilization in (**8**) is due to a longer glycosidic bond length because of a negative inductive effect of the proximal chlorine atom. Compared to (**9**), the transition state for the hydrolysis of (**8**) has better stabilization of the charge at the leaving group oxygen due to the presence of proximal chlorines.[8]

A Pd-catalysed decarboxylative Wittig reaction furnishes *c*-vinyl glycosides diastereoselectively. The Tsuji–Trost reaction, followed by the Wittig reaction, is the proposed reaction pathway. For non-pyridyl groups, *Z*-selectivity is observed as the oxaphosphetane is formed via the Newman projection (**10**), which allows for minimal gauche interactions between the sugar moiety and the aldehydic substituent (Scheme 5). The *E*-selectivity of the pyridyl group is a result of Pd–M coordination that brings the P-ylide and aldehyde into close proximity, overcoming the opposing steric factors.[9]

Sugars are introduced at the C3, C5, and C11 positions of macrolactones in a regiodivergent manner by selecting an appropriate chiral phosphoric acid catalyst or through the introduction of stoichiometric boronic acid–base additives. Mechanistic studies suggest that the reactive intermediates involved in the reaction are covalently linked anomeric phosphates rather than oxocarbenium ion pairs.[10]

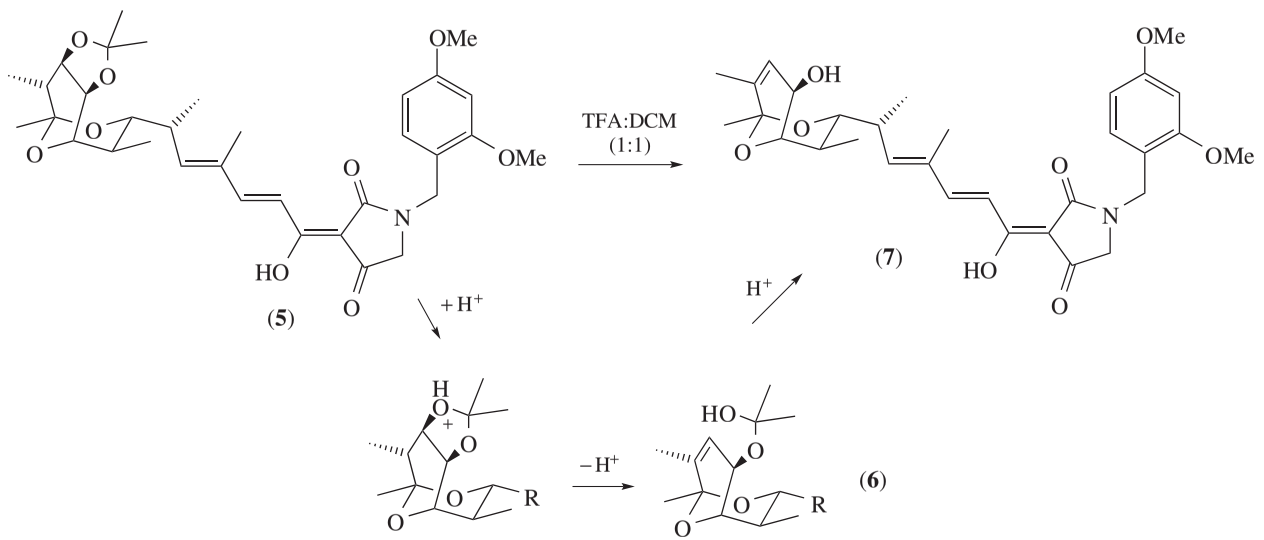

Scheme 3

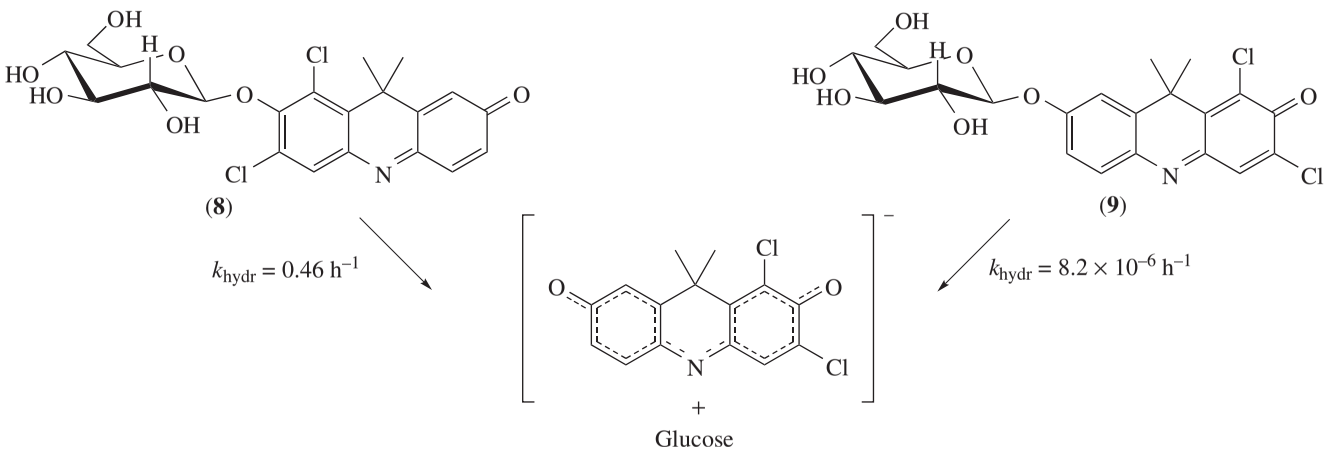
OH
H
O
HO
HO
OH
O
Cl
Cl
N
O
(8)
$k_{hydr} = 0.46\ h^{-1}$
Cl
O
O
N
Cl
+
Glucose
(9)
$k_{hydr} = 8.2 \times 10^{-6}\ h^{-1}$

Scheme 4

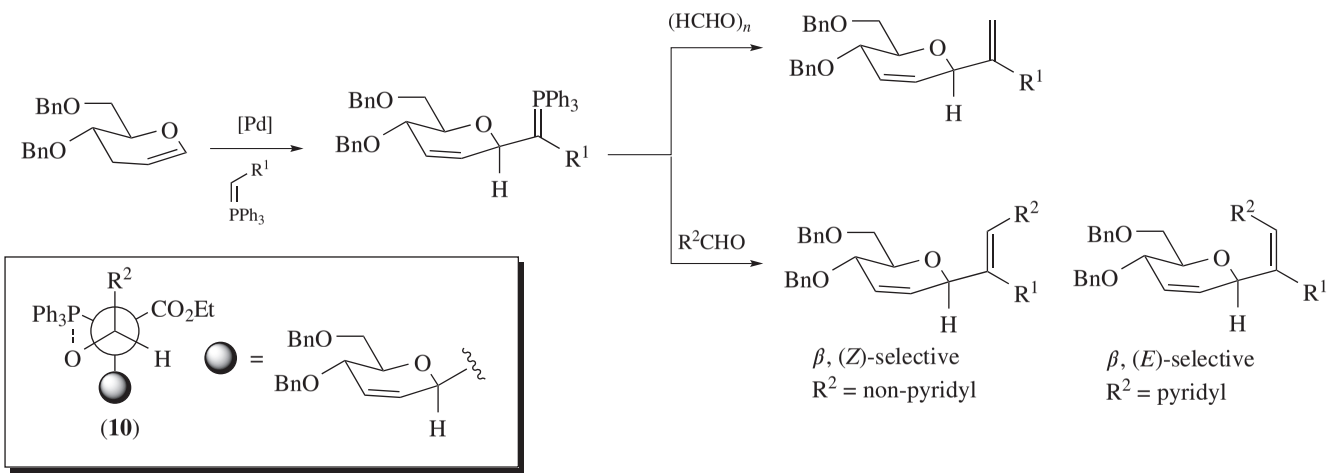
BnO
BnO
O
[Pd]
R1
PPh3
PPh3
H
R1
(HCHO)n
R2CHO
R2
Ph3P
CO2Et
O
H
(10)
=
β, (Z)-selective
R2 = non-pyridyl
β, (E)-selective
R2 = pyridyl

Scheme 5

Glycosylation of 4,6-tethered glucosides with a panel of nucleophiles reveals that decreasing electron density on glucosides or increasing electron density of nucleophilic atoms results in increasing β-selectivity. It is proposed that when the glucoside is electron deficient and the nucleophile is strong, β-selectivity occurs because the β-triflate is in equilibrium with the α-triflate which is less stable, leading to β-products. When the nucleophile is weak and the glucoside is electron rich, the triflate dissociates to form an oxocarbenium species. Nucleophilic attack from the bottom face leads to α-products through a chair-like transition state.[11]

Reactions of Ketenes

DFT calculations have been performed at the B3LYP/6-311+G(d,p) and M)6-2X/6-31(d,p) levels to understand the experimental outcome of the reaction between hydrazone (**11**) and α-oxo-ketene (**12**) (Scheme 6). Among the three possible pathways, leading to different products, the 1,3-dipolar cycloaddition is the most favoured. The mechanism is speculated to involve a 1,2-hydrogen shift that proceeds via quantum mechanical tunnelling. Without this 1,2-hydrogen shift, the other two Diels–Alder product pathways are expected to be favoured.[12]

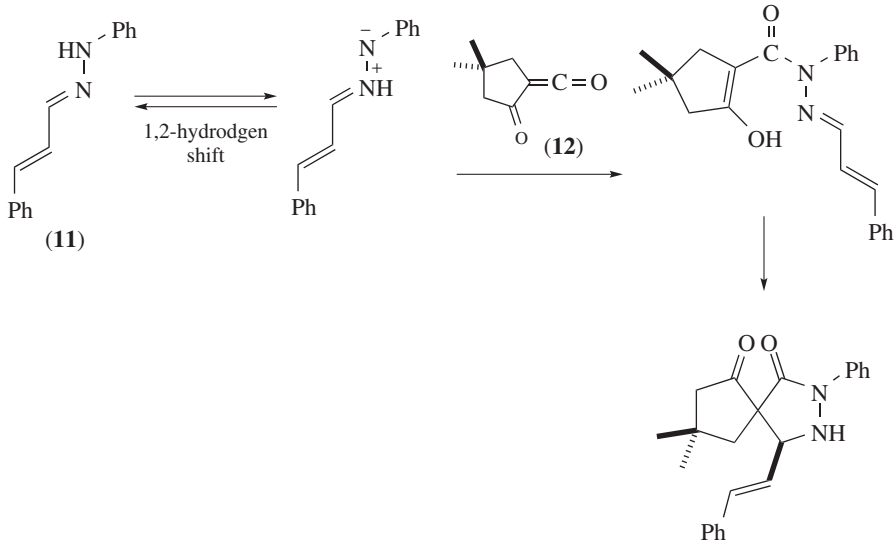

Scheme 6

The 3 + 2-cycloaddition between nitrones and ketenes has been studied using DFT and molecular electron density (MEDT). The reaction takes place in one kinetic step, but in a non-concerted mechanism. The study predicts a switch to a two-step mechanism with electrophilic ketenes.[13]

DFT methods have been used to understand the mechanism and stereochemical outcome of trimethylsilylquinine (TMSQ) or methylquinidine (MeQd)-catalysed 2 + 2-cycloaddition between methylketene (MK) and methylphenylketene (MPK). With TMSQ, *R–E* isomer is predominantly formed, while with MeQd, *S–Z* isomer is the major product. Formation of lactone occurs via a stepwise process. The enantio- and diastereo-selectivities are controlled by lower distortion of the reactants in the most preferred transition state. With $LiClO_4$ as the additive, the stereochemical outcome (*S–E* with MeQd and *R–E* with TMSQ) is due to more effective noncovalent interactions among the catalyst, substrate, and $LiClO_4$ in the transition state of the rate-determining step.[14]

(ee)
(de)

Formation and Reactions of Nitrogen Derivatives

Imines: General, Synthesis, and Iminium Chemistry

The amphiphilic imines aggregate to micelles in water. This was judged by diffusion-ordered NMR spectroscopy, dynamic light scattering, and interferometric scattering microscopy. These imines do not undergo autocatalysis and instead hydrolyse in a neutral aqueous solution.[15]

DFT (time-dependent)//CASPT2 (active space second-order perturbation theory) and CASPT2//CASSCF (complete active space-consistent field) studies shed light onto the mechanism of imine photoswitches (**13**) and (**14**) (Scheme 7). A mild energy barrier exists for $E \rightarrow Z$ and $Z \rightarrow E$ isomerization of (**13**). The photoisomerization of (**14**) is barrierless.[16]

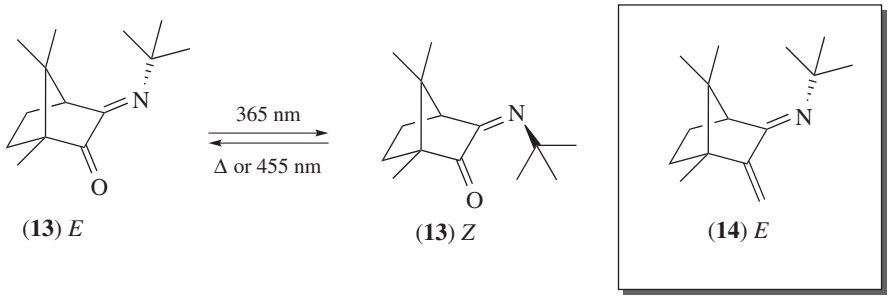

Scheme 7

Photoredox-catalysed cross-coupling of enamides and bromodifluoro compounds provides *gem*-difluoromethylenated γ-imines (Scheme 8). The mechanistic hypothesis involves a radical/SET pathway, and NMR and LC–MS analysis of the crude reaction failed to detect the H atom abstraction product of (**15**), indicating the formation of a carbocation. The radical reduces Ir(IV) into Ir(III), thus regenerating the catalyst.[17]

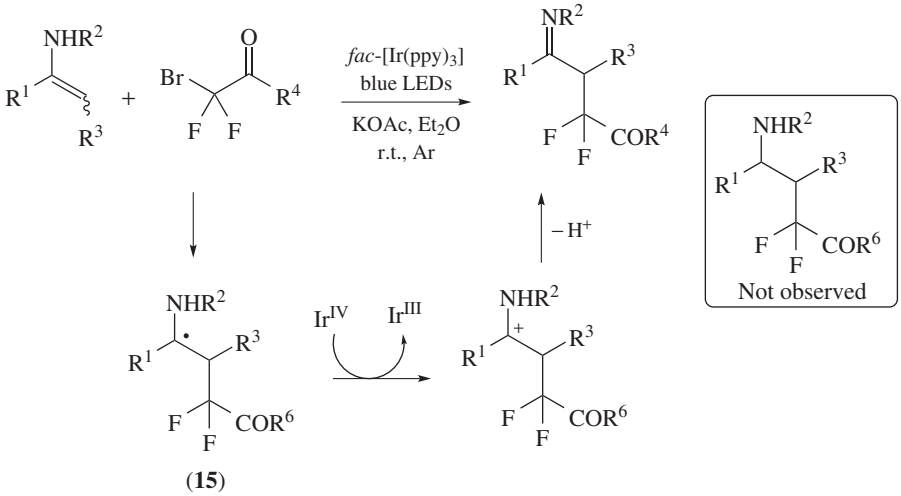

Scheme 8

Formation of ketenimines has been achieved via a decarboxylative allylic rearrangement pathway that does not require strong stabilizing or protecting groups (Scheme 9). A crossover experiment concluded that the products were formed via a dissociative solvent-separated

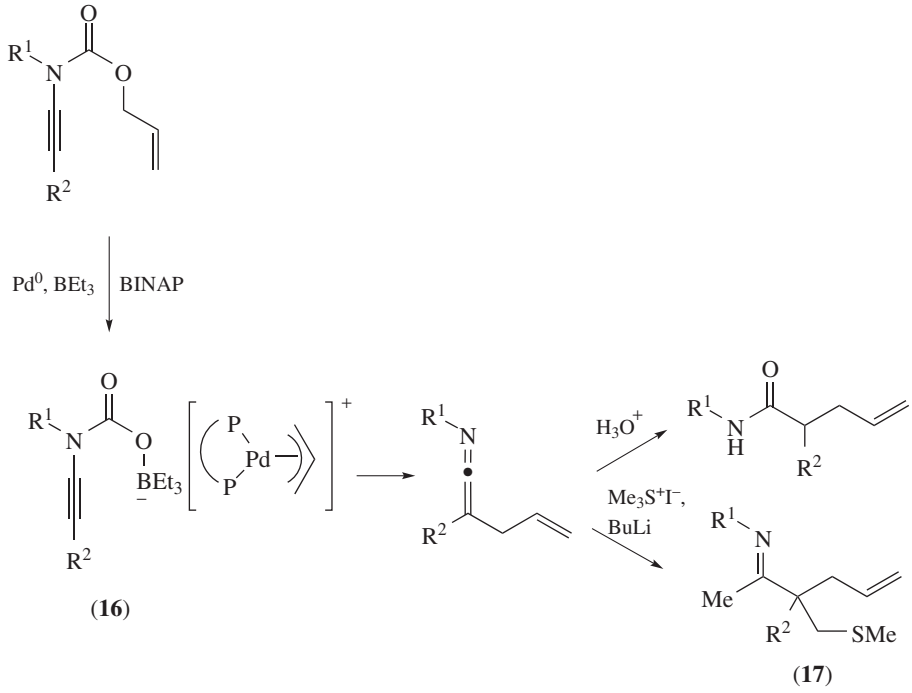

(**16**)

(**17**)

Scheme 9

ion pair (**16**). Kinetic studies and the presence of the bidentate ligand on the Pd alongside the allylic intermediate suggested that the reaction goes through an outer-sphere process in which reductive alkylation is rate limiting. Owing to the labile nature of ketenimines, they were immediately hydrolysed to amides or reacted with sulfur ylides to form imines. Formation of imine (**17**) is proposed via nucleophilic addition to the central carbon of the ketenimine, followed by C-to-N proton transfer, [2,3]-Wittig rearrangement, and subsequent tautomerization.[18]

DFT calculations indicate that H abstraction from (**18**) by most radicals is the lowest-barrier mechanism (Scheme 10). A subsequent N–N β-scission leads to the formation of the imine.[19]

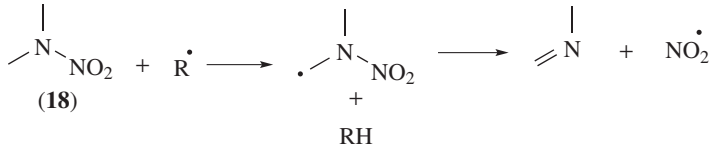

(**18**)

Scheme 10

DFT is used to study the regio- and diastereo-selectivity of Rh(III)-catalysed cyclization reactions of *N*-arylnitrones. The regioselectivity is controlled by the electronic effect in alkyne insertion. The diastereoselectivity is controlled by the imine insertion step.[20]

Active transition states in the (*R*)-TRIP-catalysed reactions of imines are identified by determining the impact of photoisomerization of double bonds on the rate and the *ee* of the reaction. The method, named decrypting transition state by light (DTS–*hν*), identified Type I *Z* and Type II *Z* (Type I = bottom nucleophilic attack; Type II = top nucleophilic attack; *E* and *Z* are the diastereomers of imines) pathways to be competing in the asymmetric transfer

hydrogenation of ketimines. Type I *E* and Type II *E* pathways are active in the nucleophilic addition of acetylacetone to *N*-Boc-protected aldimines. Quantum chemical calculations and noncovalent interaction analysis support these experimental findings.[21] (de)

The regioselective cycloaddition of aromatic aldehydes and *gem*-difluoro azomethine ylides (**19**) provides difluoropyrrolidine cycloadducts (**20**) that hydrolyse under the reaction conditions to give oxazolidin-4-ones (**21**) (Scheme 11). Correlation analysis and DFT calculations reveal a stepwise mechanism. Exchange of germinal fluorines with hydrogen results in the mechanism becoming pericyclic. The stability of cycloadducts can be increased, and fluorinated products could be isolated if the aldehydes are replaced with trifluoroacetophenone.[22]

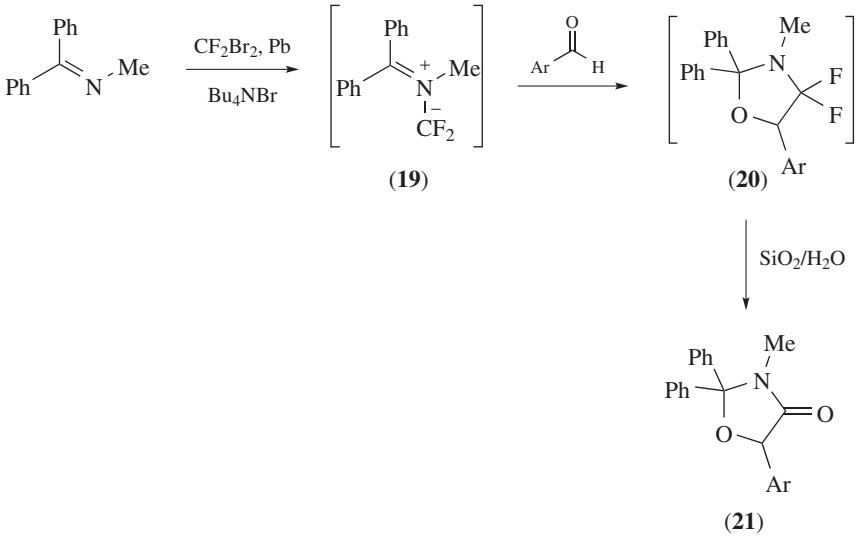

Scheme 11

Kinetic *anti*-*β*-aminonitriles can be prepared by deprotonation of secondary alkane nitriles with BuLi and addition to aryl imines. Thermodynamic *syn*-*β*-aminonitriles can be prepared by replacing BuLi with LHMDS. Use of LHMDS results in a reversible protonation of the reaction intermediate, giving *syn* product. Crossover and additional mechanistic experiments suggest that the reversible protonation mechanism is operative at −78 °C, while a (with both bases) retro- then re-addition pathway is present at rt. The later pathway results in a mixture of diastereomers.[23] (de)

Instead of the expected 3 + 2-dipolar cycloaddition, the Lewis acid-catalysed reaction of azomethine imines and nitrones to *N*-vinylpyrroles proceeds by a formal 3 + 3-cycloaddition. It is proposed that the 1,3-dipole reacts as an electrophile as a result of Lewis acid coordination. Nucleophilic attack by pyrrole, [1,7]-H-shift, followed by cyclization, leads to the final products.[24]

A rare 2 + 2-cycloaddition of carbodiimides is speculated to be operative for the synthesis of (**25**) bearing two radical groups (Scheme 12). First, the aza-Wittig reaction of bis(iminophosphorane) (**22**) with paramagnetic isocyanate (**23**) produces the intermediate (**24**). The bis(carbodiimide) intermediate (**24**) undergoes cycloaddition reaction producing (**25**).[25]

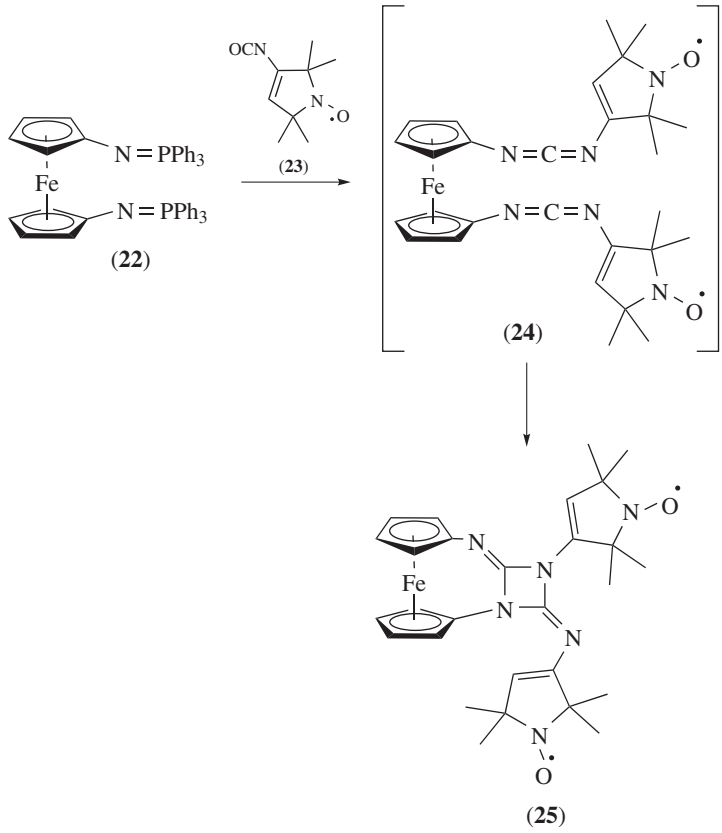

Scheme 12

Mannich, Mannich-type, and nitro-Mannich Reactions

A cascade of Staudinger/aza-Wittig/Mannich reactions of substituted oxindoles provides spiro[pyrrolidine-3,3′-oxindoles]. The stereochemical outcome is hypothesized to be due to pseudoequatorial location of C2′ and C5′ groups in the Mannich step transition state.[26]

Other 'Name' Reactions of Imines

The mechanism of a quinine-squaramide-catalysed enantioselective aza-Friedel–Crafts reaction between (**26**) and (**27**) is studied using DFT (Scheme 13). The C–C bond-forming step is the rate-determining step. The *R*-configuration adduct is energetically and kinetically favoured. The nucleophile is activated by the squaramide N–H groups and the electrophile binds to the protonated amine of the catalyst.[27]

Alkylations

A photoredox/Brønsted acid cocatalysis enables radical alkylation of imines with 4-alkyl-1,4-dihydropyridine (**28**) (Scheme 14). The reaction is terminated by the addition of TEMPO, and the TEMPO-trapped product is identified by LC–MS. In one experiment, a dimeric product is isolated. Stern–Volmer quenching experiments show significant quench of one photocatalyst's fluorescence by (**28**) and a much lower effect by the imine. On the basis of these observations,

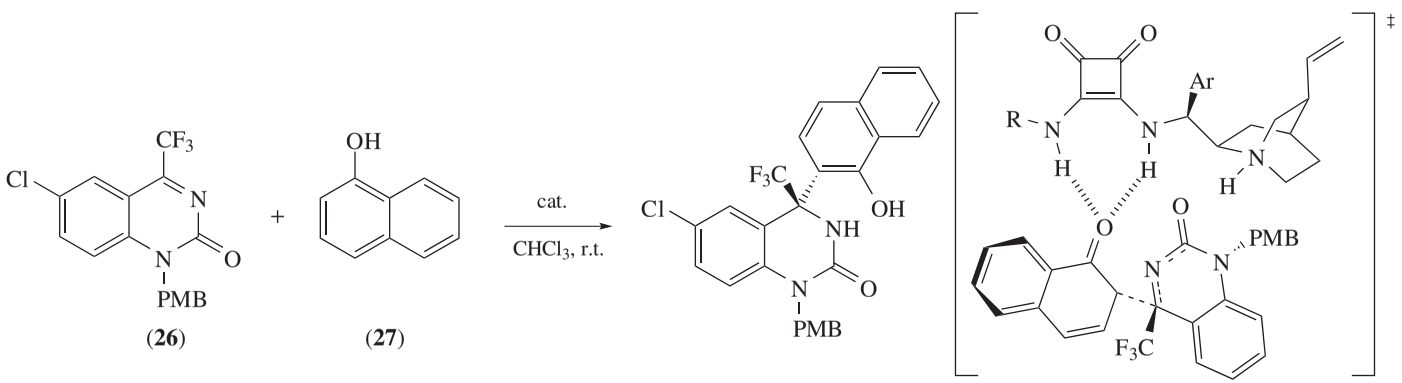
CF3
Cl
N
N
O
PMB
(26)
+
OH
(27)
cat.
CHCl3, r.t.
F3C
OH
Cl
NH
N
O
PMB
O
O
R
N
H
N
H
Ar
N
H
O
O
N
N
PMB
F3C
‡

Scheme 13

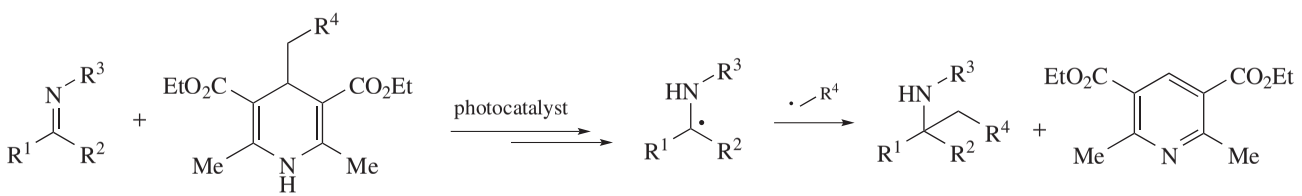
R4
N
R3
R1
R2
+
EtO2C
CO2Et
Me
N
H
Me
photocatalyst
HN
R3
R1
R2
R4
HN
R3
R1
R2
R4
+
EtO2C
CO2Et
Me
N
Me

(**28**)

Scheme 14

a mechanistic cycle is proposed, which involves the formation of an alkyl radical from and its reaction with the alkylamine radical.[28]

Miscellaneous Additions to Imines

Thermal intramolecular cyclization of *N*-aryloxyacrylate aldimines (**29**) leads to the synthesis of functionalized dihydrobenzoxazoles (**30**) (Scheme 15). An intramolecular attack on the conjugated double bond, followed by the ring opening and closure, leads to the product formation. Mechanistic studies exclude the possibility of (**31**) an aza-Michael addition to the α,β-unsaturated ester. A crossover experiment confirms the intramolecular nature of the rearrangement. The successful formation of (**30**) in the presence of TEMPO is used to exclude the participation of radicals in this reaction.[29]

Electrochemical, spectroscopic, computational, and kinetic studies provide understanding of the factors governing the iminium ion-mediated enantioselective radical conjugate addition to β,β-disubstituted cyclic enones. The investigation revealed that the turnover-limiting step is the single-electron transfer reaction (SET).[30]

Propylphosphonic anhydride (T3P®) mediates a three-component Ugi-type reaction, providing α-amino amides. The anhydride T3P® is speculated to promote the formation of the imine, its protonation, and the formation of (**32**) (Scheme 16).[31]

A Ugi/Staudinger/aza-Wittig sequence provides a 3,4-dihydroquinazoline (**34**). It is proposed that the Ugi-type reaction of isocyanide, acid, aldehyde, and amine produces an azide intermediate, which reacts with PPh_3 by a Staudinger reaction generating the intermediate (**33**) (Scheme 17). The iminophosphorane intermediate (**33**) undergoes an aza-Wittig reaction, producing (**34**). The observed regioselectivity is attributed to be a result of greater reactivity of the sterically less-hindered carbonyl group.[32]

A one-pot Ugi-3CR/Wittig sequence provides indoles (Scheme 18). This is first time isocyanide-substituted phosphonium salts are used in the Ugi reaction. Although no intermediates are isolated, intermediate (**35**) is expected to be involved in the reaction mechanism.[33]

Acetaldehyde and ammonia react to form 2,4,6-trimethyl-1,3,5-hexahydrotiazine trihydrate. DFT calculations suggest that the most favourable pathway for the formation of the cyclic triazine product is a result of the repetition of the following stages: addition of a primary amine acetaldehyde, dehydration to produce imine, and the addition of ammonia to form the germinal diamine.[34]

Oxidation and Reduction of Imines

DFT and ONIOM (B3LYP/6-31G**: UFF) calculations show that the presence of an *ortho*-hydroxyl group on the imine results in the transfer hydrogenation reaction to proceed through a 14-membered bifunctional mechanism. On the basis of the transition state, a qualitative model is proposed for predicting the stereoinduction in this reaction. Contrary to conventional models, the new model predicts a minimal increase in steric repulsion between the large group on the imine nitrogen and the $SiPh_3$ group on the catalyst.[35]

Phosphorus triamide (**36**) reacts with pinacolborane via B–H bond activation, providing (**37**) (Scheme 19). P-Hydrido-1,3,2-diazaphospholene (**37**) shows hydridic reactivity and it reacts with imines. The intermediates (**38**) eliminate the *N*-borylamine product via an intramolecular boryl transfer. The proposed mechanism is verified by kinetic experiments and by independently verified stoichiometric steps.[36]

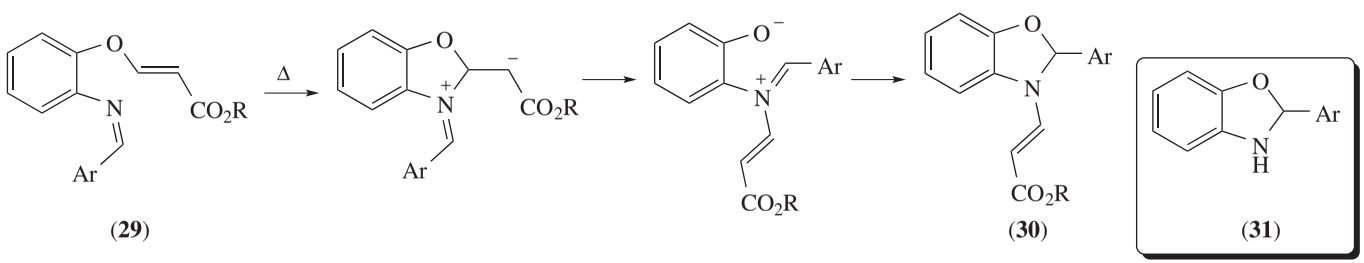

Scheme 15

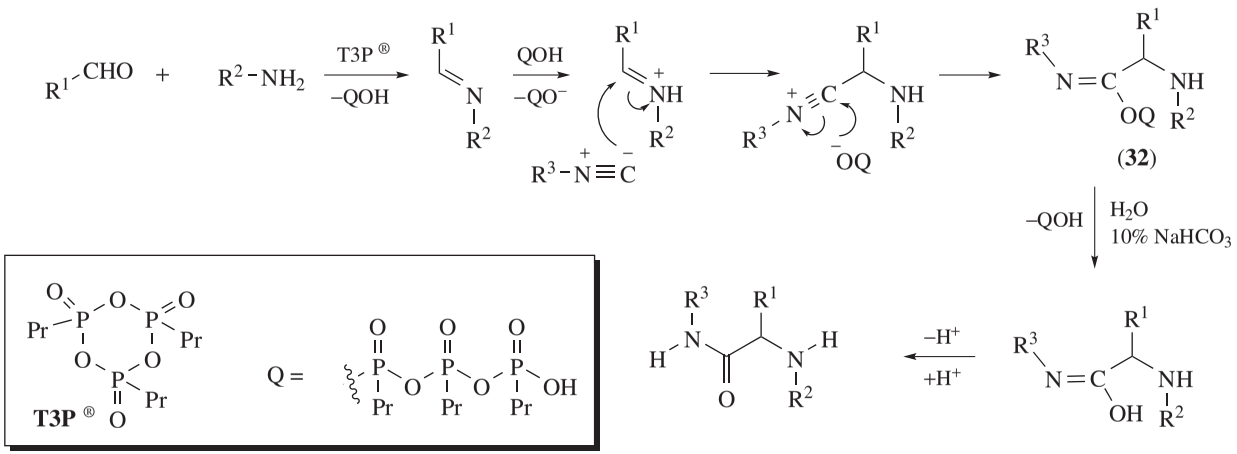

Scheme 16

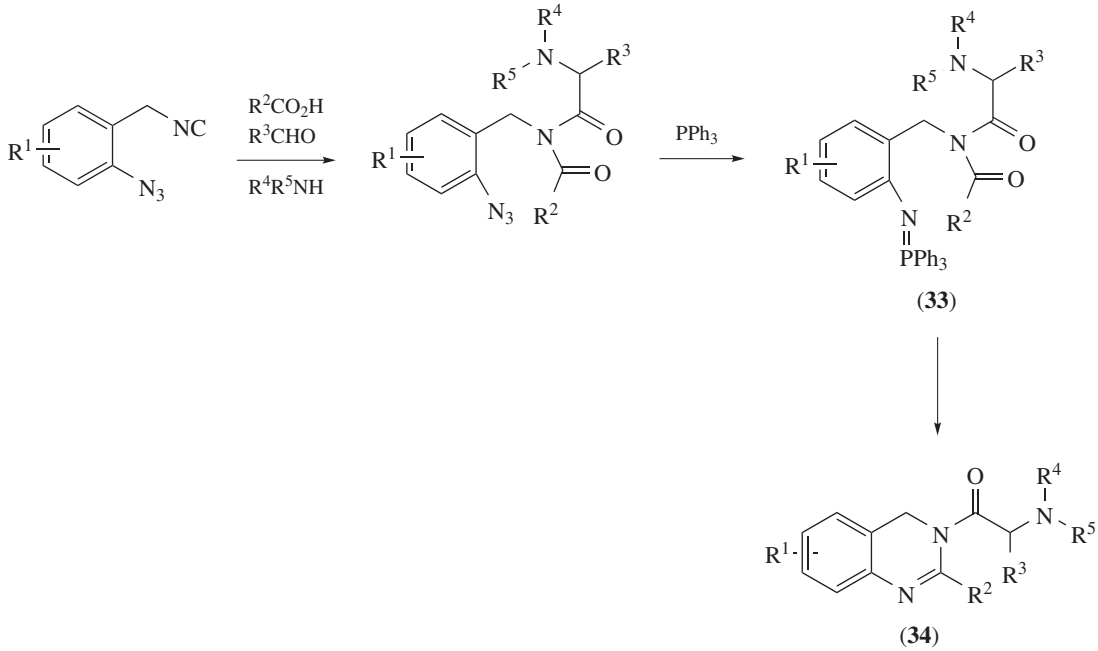

Scheme 17

Catalytic activity of 1,2,4,3-triazaphospholenes (TAPs) is evaluated in the hydroboration of imines and α,β unsaturated aldehydes. DFT supports a mechanism in which the transition state of the rate-determining step involves a triazaphospholene cation that interacts with the substrate.[37]

Amides are prepared from aldimines via an aerobic oxidative NHC catalysis, which also involves the use of LiCl as a cooperative Lewis acid catalyst (Scheme 20). The mechanism involves the aza-Breslow intermediate (**39**), which was isolated under inert conditions. The intermediate could be converted into the corresponding amide under the reaction conditions.[38]

A Cu(II)/O_2-catalytic system provides oxidative N-dealkylation of *N*-(2-pyridylmethyl)phenylamine and its derivatives. Mechanistic studies show that the imine and amide species are possible precursors, leading to the carboxylate.[39]

Other Reactions of Imines

Reaction of 2-picolylamine and benzaldehyde gives cyclized product (**40**) (Scheme 21). The unexpected formation of (**40**) is explained as a result of transamination/transimination (TATI), which provides (**41**). Condensation of benzaldehyde with (**41**) provides (**42**). As a result of lability of the pyridine ligand, (**42**) is converted into the (**43**), which upon cyclization provides (**44**). Tautomerization of (**44**) gives (**45**) which, owing to steric repulsion between hydrogen atoms of the pyridine units, loses the metal, forming (**40**).[40]

A mechanistic model, based on steric effects, is proposed to rationalize the observed diastereoselectivity in thioketene–imine cycloaddition. However, it is shown that epimerization of products is facile under the reaction conditions. Therefore, it is unclear if the model has any use in predicting the outcome of a reaction.[41]

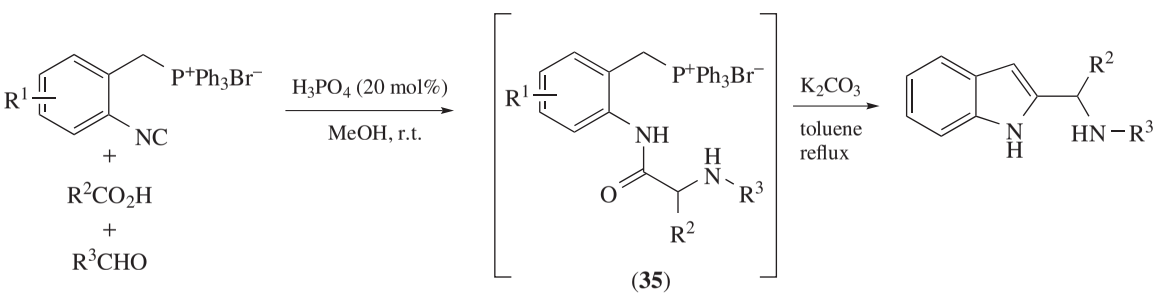
R1
P+Ph3Br−
NC
+
R2CO2H
+
R3CHO
H3PO4 (20 mol%)
MeOH, r.t.
NH
O
H
N
R3
R2
(35)
K2CO3
toluene
reflux
R2
N
H
HN−R3

Scheme 18

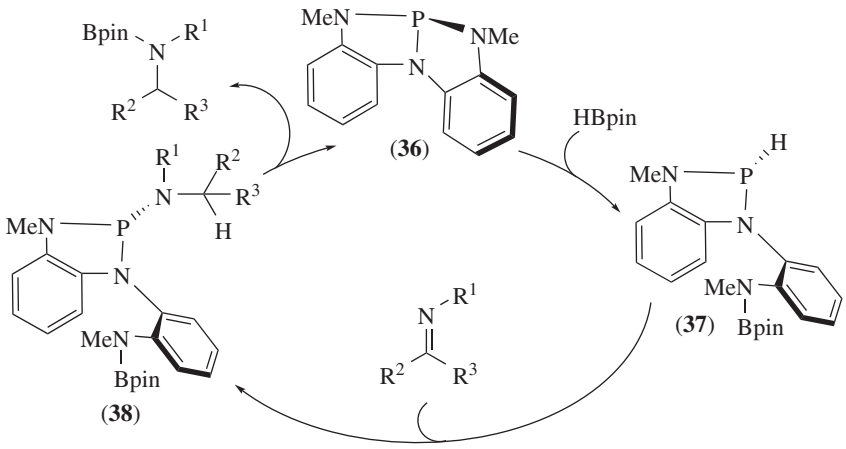

Scheme 19

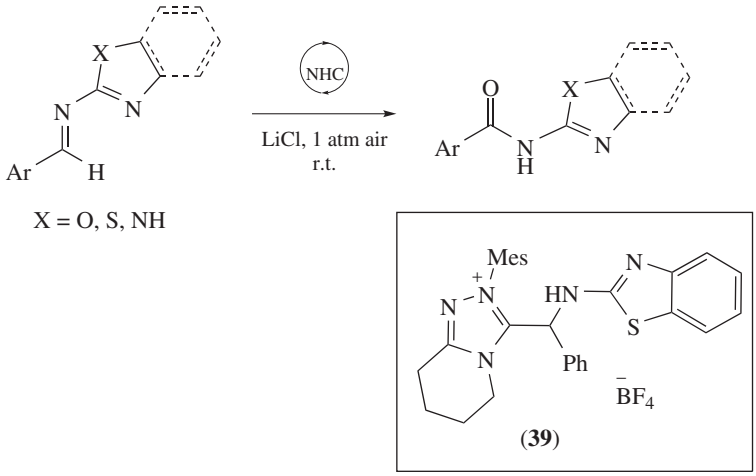

Scheme 20

Enantioselective [4 + 1]-annulation between *α,β*-unsaturated imines and allylic carbonates can be catalysed by a hybrid *P*-chiral phosphine oxide–phosphine (Scheme 22). A model is proposed to explain the enantioselectivity. The *in situ* generated P-ylide (**46**) forms a cyclic structure due to coulombic interactions. The smaller (Ph) group of the catalyst is positioned upward, while the anisole points downward. The bond formation happens from the *Si* face where the sterically less-demanding Ph group is present.[42] (ee)

A small-ring phosphacycle (**47**) catalyses deoxygenative N–N bond-forming heterocyclization in the presence of hydrosilane (Scheme 23). Phosphorus NMR and DFT calculations suggest that the reaction mechanism proceeds via a turnover-limiting [3 + 1] reaction between nitroarene and the catalyst. Strain/distortion analysis of the [3 + 1] transition state shows that the geometric constraints in (**48**) result in the lowering of LUMO (compared with the transition state for an acyclic phosphorus catalyst), which preferentially permits synergistic HOMO–LUMO interactions between the two coupling partners.[43]

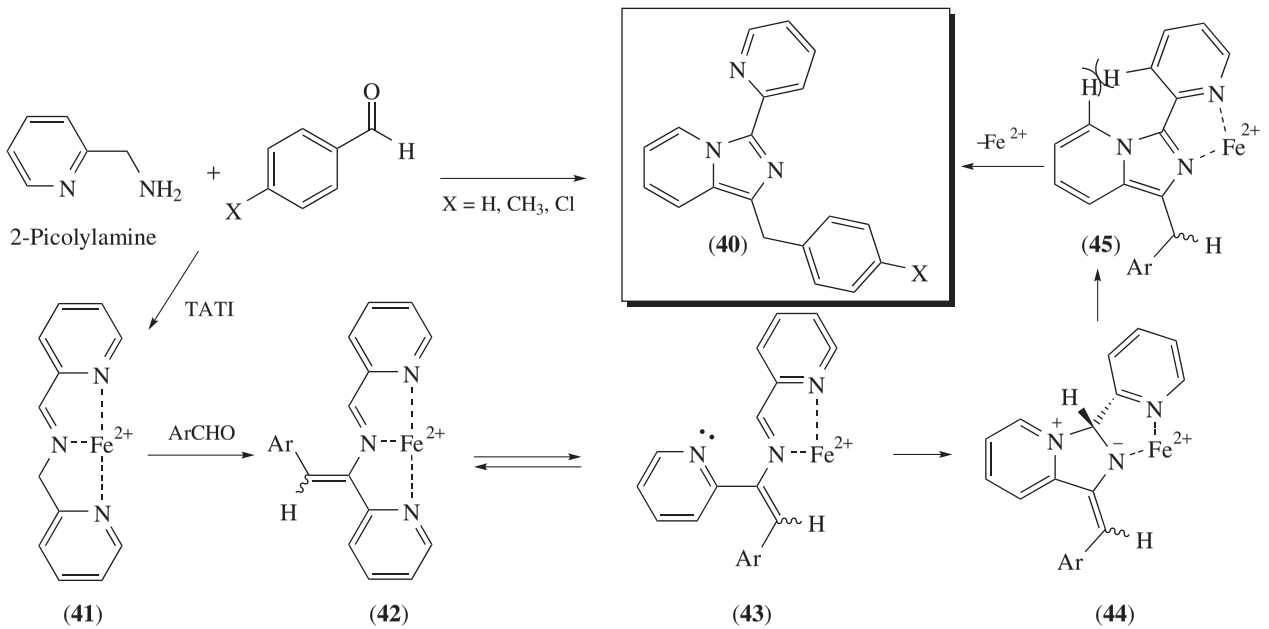

Scheme 21

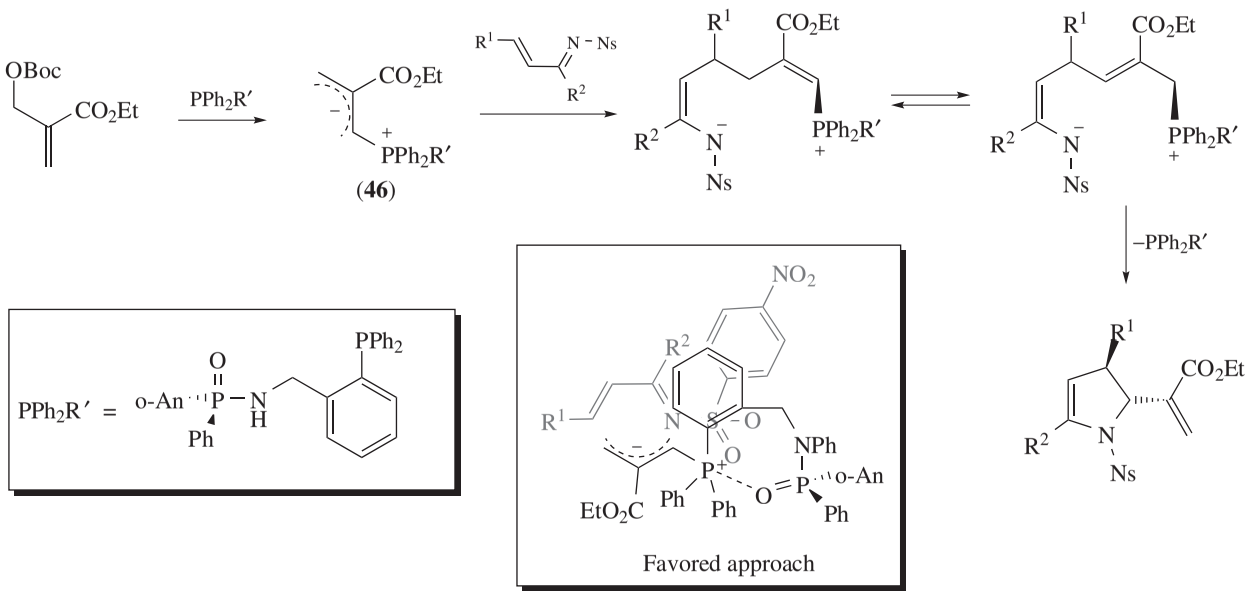
OBoc
CO2Et
PPh2R′
CO2Et
PPh2R′
(46)
R1
N – Ns
R2
R1
CO2Et
R2
N
Ns
PPh2R′
–PPh2R′
PPh2R′ =
o-An
P
O
N
H
Ph
PPh2
NO2
R2
R1
N
S
O
O
NPh
P
o-An
EtO2C
Ph
Ph
O
P
Ph
Favored approach

Scheme 22

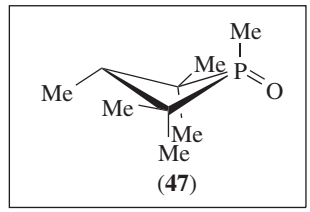

(**47**)

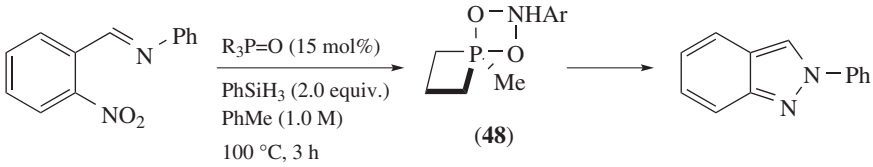

(**48**)

Scheme 23

An unexpected formation of bicyclic phosphonate (**49**) is proposed to be a result of azomethine ylide formation, followed by a cyclization with acylphosphonates (Scheme 24). The alternative mechanism involving the ylide formation via condensation of proline with acylphosphonates is discounted as it should give a different product.[44]

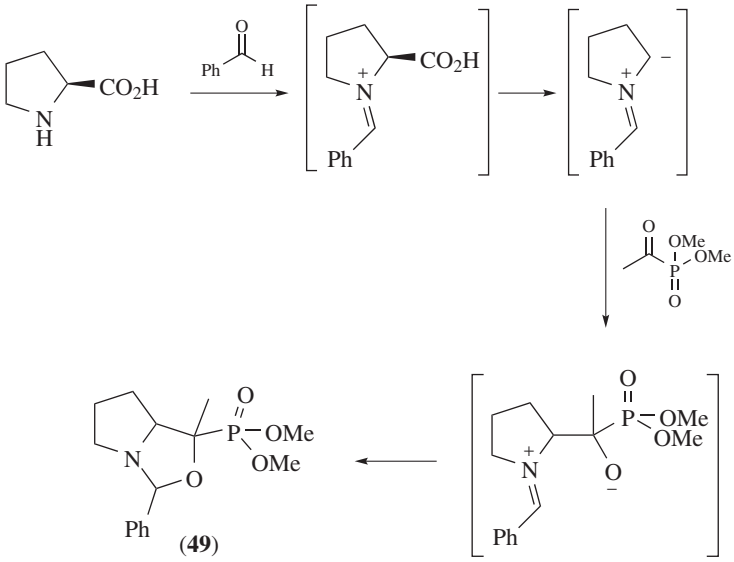

(**49**)

Scheme 24

A DFT study of asymmetric induction in Nazarov reactions shows that a chiral vicinal diamine (**50**) forms an enamine–iminium adduct (**51**) with α-ketoenones (Scheme 25). Adduct (**51**) undergoes a conrotatory electrocyclization process, yielding the stable intermediate (**52**). The six-membered ring in (**51**) favours one mode of helicity of the electrocyclization transition state, thus providing the stereocontrol. As (**52**) is extremely stable, it causes product inhibition when diamine is used in substoichiometric quantities. Hydrolysis of intermediate (**52**) via acidic workup provides the cyclized product (**53**).[45]

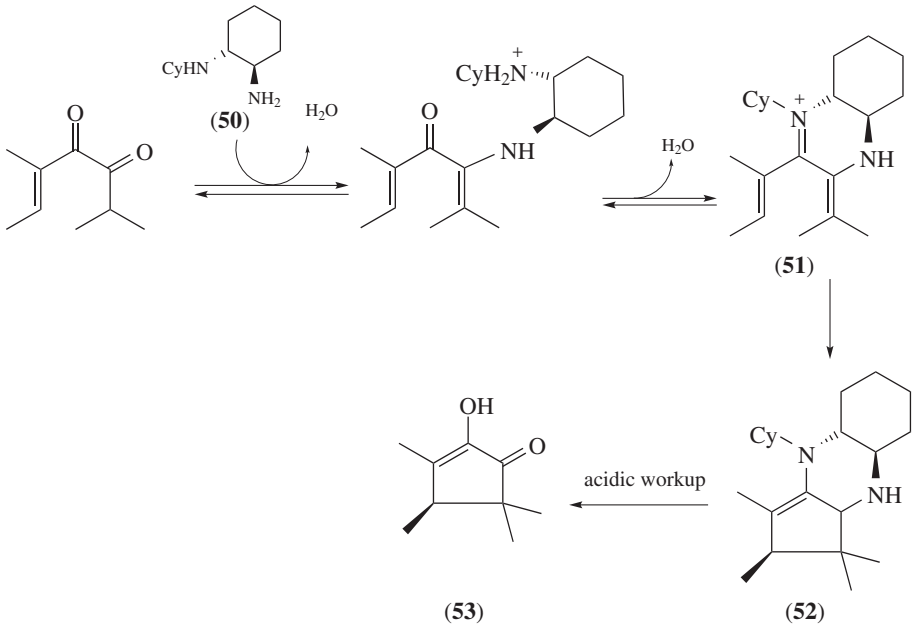

Scheme 25

Oximes, Hydrazones, and Related Species

The radiation chemical behaviour of butanal oxime is investigated for its applicability as a replacement of hydrazinium nitrate in nuclear fuel processing. In a ternary (water–nitric acid–butanal oxime) solution, butanal oxime behaviour is influenced by the nitric acid concentration. At a low nitric acid concentration ($\leq 0.5\,mol\,L^{-1}$), butanal oxime is protected by nitrate ions toward the scavenging of hydrogen and hydroxyl radicals (generated because of radiolysis of water). At this concentration, it is in competition with hydrogen peroxide (one of water radiolysis products) to reduce HNO_2 and is, therefore, protected by hydrogen peroxide. At higher concentrations of nitric acid ($\geq 0.5\,mol\,L^{-1}$), HNO_2 accumulates in the medium, leading to butanal oxime degradation via an autocatalytic oxidation process.[46]

Poly(oxime-urethanes) (POUs) can be prepared from uncatalysed polyaddition of multifunctional oximes and hexamethylene diisocyanate. The oxime-urethane structures are reversible at about 100 °C through oxime-enabled transcarbamoylation via thermal dissociation. Density function theory calculations show that the fast oxime-urethanation and thermoreversibility of POUs is mediated by the nitrone tautomer of the oxime.[47]

Condensation of arylamines and β-ketooximes, followed by metal-free, acid-catalysed N-arylation, results in the formation of functionalized quinoxalines. Radical inhibitors do not significantly affect the reaction, and the desired product is not obtained when the OH of oxime was replaced by OMe.[48]

Cyclohexanone oximes are converted into primary anilines by utilizing a heterogeneous Mg–Al-layered double hydroxide-supported Pd catalyst ($Pd(OH)_x$/LDH). Controlled experiments and kinetic studies show that the reaction proceeds through a dehydration/dehydrogenation sequence involving a concerted catalysis of the LDH and the Pd species present on the surface of LDH.[49]

A dehydrogenation/hydration sequence gives access to (**54**), which undergoes Lossen rearrangement providing (**55**), a key intermediate in the synthesis of BMS-955176 (Scheme 26).[50]

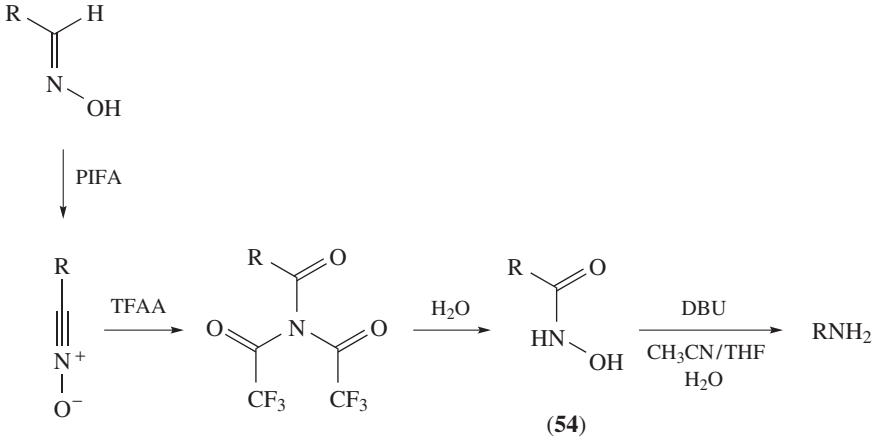

(**54**)

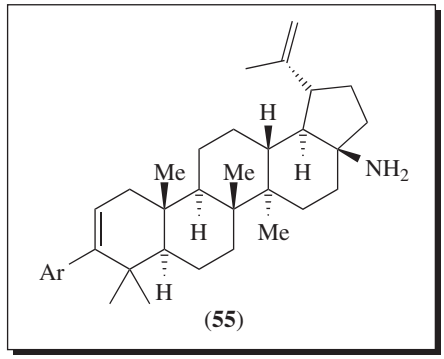

(**55**)

Scheme 26

DFT calculations suggest that the α-ketoacid-hydroxylamine amide-forming reaction involves a concerted migration of (N–OH) to the adjacent carbon in one of the key steps. In the case of *O*-Bz-substituted hydroxylamines, simultaneous loss of CO_2 and the benzoate group from the hemiaminal intermediate leads to the formation of the product.[51]

Aromatic thiols and thioacetic acid are used as nucleophilic catalysts in the isomerization of C=N bond in acylhydrazones. Thiols can be oxidized into catalytically inactive disulfides, and disulfides can be reduced into catalytically active thiols. Therefore, the isomerization can be controlled via the oxidation of the catalyst. This approach, combined with the UV irradiation, is used to control $E \rightarrow Z$ or $Z \rightarrow E$ isomerization.[52]

An enantioselective synthesis of γ-lactams is realized via an NHC-catalysed [4 + 2] annulation of 2-bromo-2-enals. The proposed catalytic cycle includes formation of Breslow's intermediate, debromination, enolate formation, and its formal 4 + 2-cycloaddition with acylhydrazone. The subsequent elimination of the product regenerates the catalyst.[53]

Theoretical investigations on the NHC-catalysed γ-C–H deprotonation/functionalization of α,β-unsaturated esters with hydrazones show that the reaction goes through a mechanism where NHC acts as a nucleophilic catalyst. The [4 + 2]-cycloaddition of dienolate with hydrazone is the stereoselectivity-determining step, and *R*-configured products are preferred. The NHC strengthens the acidity and electrophilicity to promote the deprotonation, showing that it is not the usual NHC-catalysed umpolung carbonyl reaction.[54]

A metal-free 2 + 1 + 2-cycloaddition between tosylhydrazones and hexahydro-1,3,5-triazines (**56**), which collapse to imine (**57**), in the presence of $LiOBu^t$, provides imidazolidines (Scheme 27). Deuterium-labelling experiments and crossover experiments suggest that $LiOBu^t$ plays a dual role in the reaction by generating the diazo compound and promoting the cycloaddition.[55]

The addition of chiral biphenols-catalysed asymmetric boronate to sulfonyl hydrazones gives chiral hydrazines (Scheme 28). This may eliminate sulfinic acid, forming diazene intermediate, which by retro-ene reaction provides allenes (**58**) or (**59**).[56]

Ketones and H-phosphine oxides form *β*-ketophosphine oxides by a copper-catalysed reaction (Scheme 29). Control experiments and labelling studies suggest a radical pathway in which the ketone oxygen in the product comes from O_2. In the proposed mechanism, the ketone is converted into a vinylhydrazinedicarboxylate (**60**). In the presence of Cu(II), O_2, and Et_3N, (**61**) is converted into (**62**). The P-radical reacts with (**60**) producing (**63**), which after radical reaction, elimination, and tautomerization gives the product. Intermediates (**62**), (**63**), (**64**), and by-product (**65**) were all detected by LC–MS.[57]

An intramolecular propargylic ene reaction, followed by a Diels–Alder reaction of *N*,*N*-dimethylhydrazones and oximino ethers, is used for the preparation of polycyclic pyridine derivatives. The overall process is a formal 2 + 2 + 2-cycloaddition. No reaction happens when the intermolecular version of this reaction is attempted, indicating the exceptional reactivity of vinylallenes generated in the intramolecular reaction due to the highly reactive s-*cis* conformation.[58]

DFT calculations and kinetic studies suggest that the heteroisomerization reaction of ketone (**66**) is catalysed by trace copper salts and that *Z*- to *E*-hydrazone isomerization occurs through an enehydrazine intermediate (**67**) (Scheme 30). The *E* hydrazone undergoes a rate-determining cyclization, providing aminopyrrole products.[59]

A Pd-catalysed cross-coupling reaction of a benzoyl bromide with *N*-tosylhydrazones, followed by an intramolecular Heck reaction with aryl bromide, gives (**68**) (Scheme 31). A *syn*-carbopalladation, followed by a *syn*-*β*-hydride elimination, is proposed to explain the observed stereochemistry.[60]

A transition-metal and base-free coupling reaction of *N*-tosylhydrazones with 1,3-dicarbonyl compounds gives tetraketo compounds (Scheme 32). The postulated mechanism involves nucleophilic addition of dimedone to *N*-tosylhydrazone, which leads to the intermediate (**69**). Intramolecular decomposition of (**69**) gives enone (**70**). The 1,4-addition of dimedone on enone (**70**) provides the product. When the *N*-tosylhydrazone is derived from cinnamaldehyde, the enone is isolable.[61]

A two-step, one-pot transformation provides access to *N*-substituted-2*H*-indazol-2-amine derivatives. Imine formation, followed by Cadogan reaction, provides these products. *para*-Substitution of the aromatic ring with the electron-donating group results in the formation of amines. The formation of an amine is suspected to be due to nitrene stabilization by electron-donating groups in the cyclization step, which hinders in an efficient reductive cyclization.[62]

An asymmetric anionic amino-Cope rearrangement is reported. The enamide intermediate reacts with an electrophile in a domino sequence. If an electrophilic site is present, it can lead to cyclized products. DFT calculations suggest a stepwise mechanism. The stereochemical outcome is explained as a result of the transition state in which the sulfur and nitrogen lone pairs are *anti* to one another, thus avoiding lone pair repulsion. In the presence of an *α*-substituent, the enamide cyclization can be suppressed. Interestingly, in this scenario, the new stereocentre possesses the opposite stereochemistry.[63]

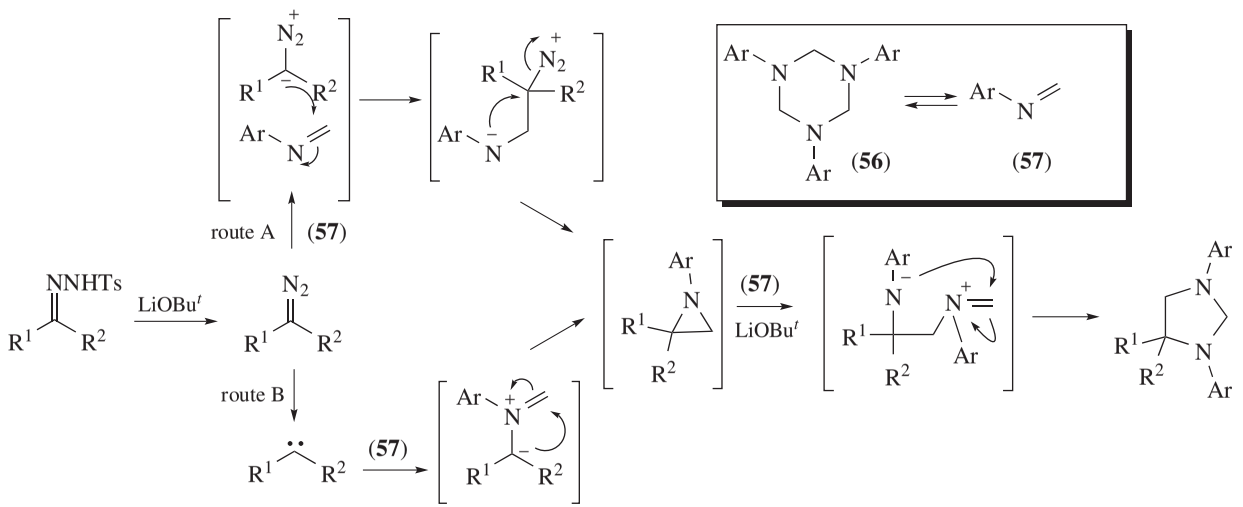

Scheme 27

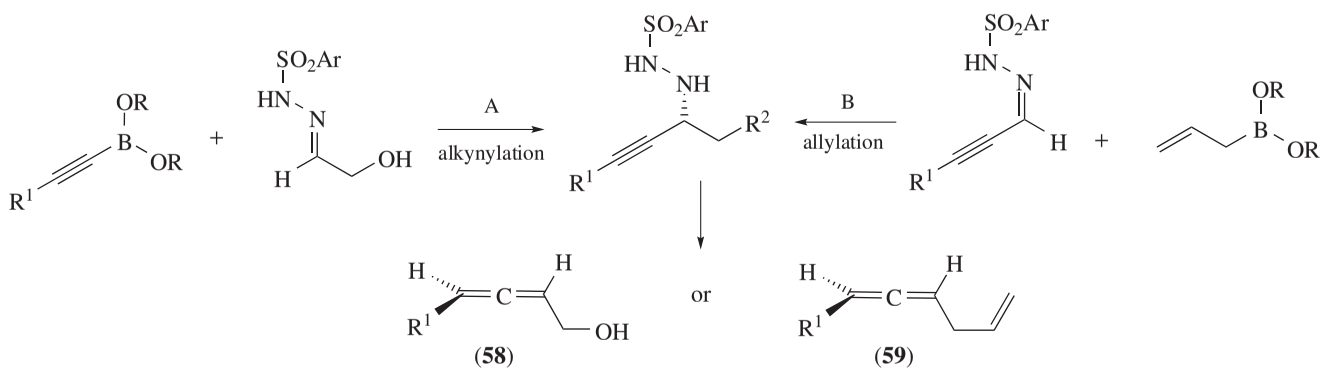
OR
B
OR
R1
+
SO2Ar
HN
N
H
OH
A
alkynylation
SO2Ar
HN
NH
R2
R1
B
allylation
SO2Ar
HN
N
H
R1
+
OR
B
OR
H
H
C
R1
OH
(58)
or
H
H
C
R1
(59)

Scheme 28

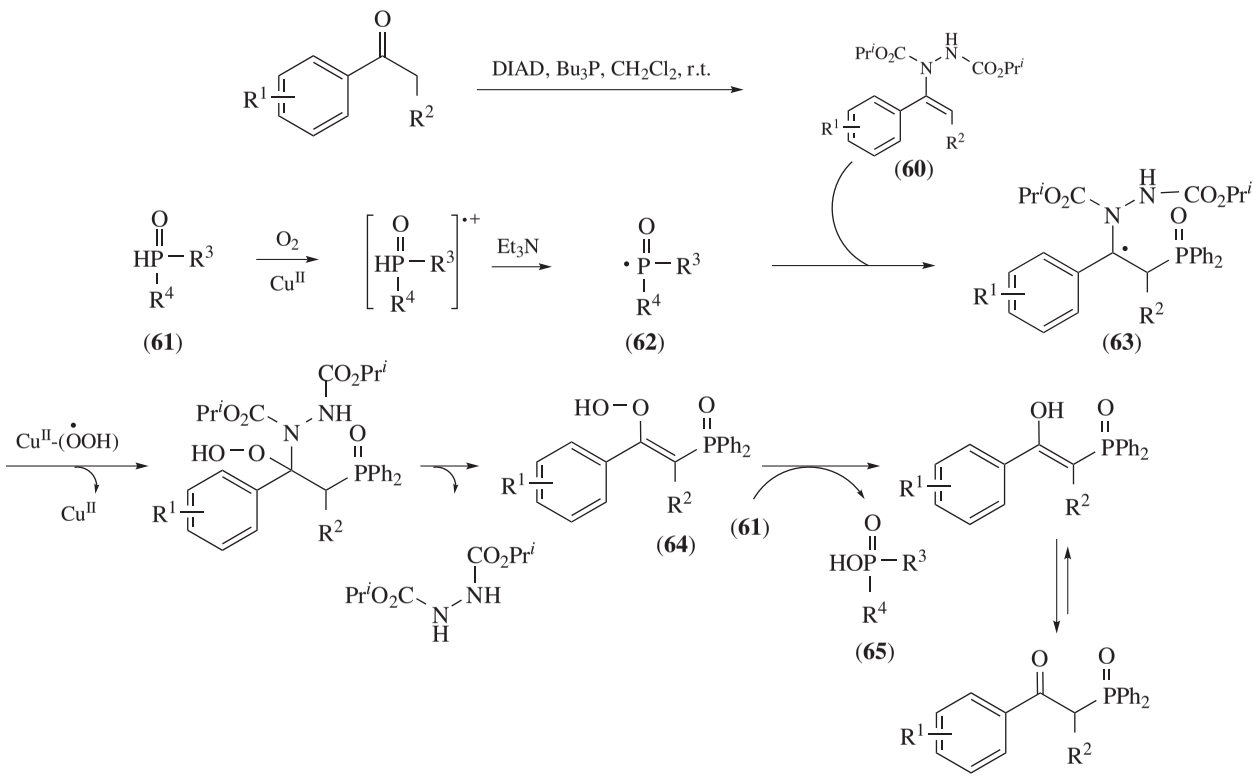

Scheme 29

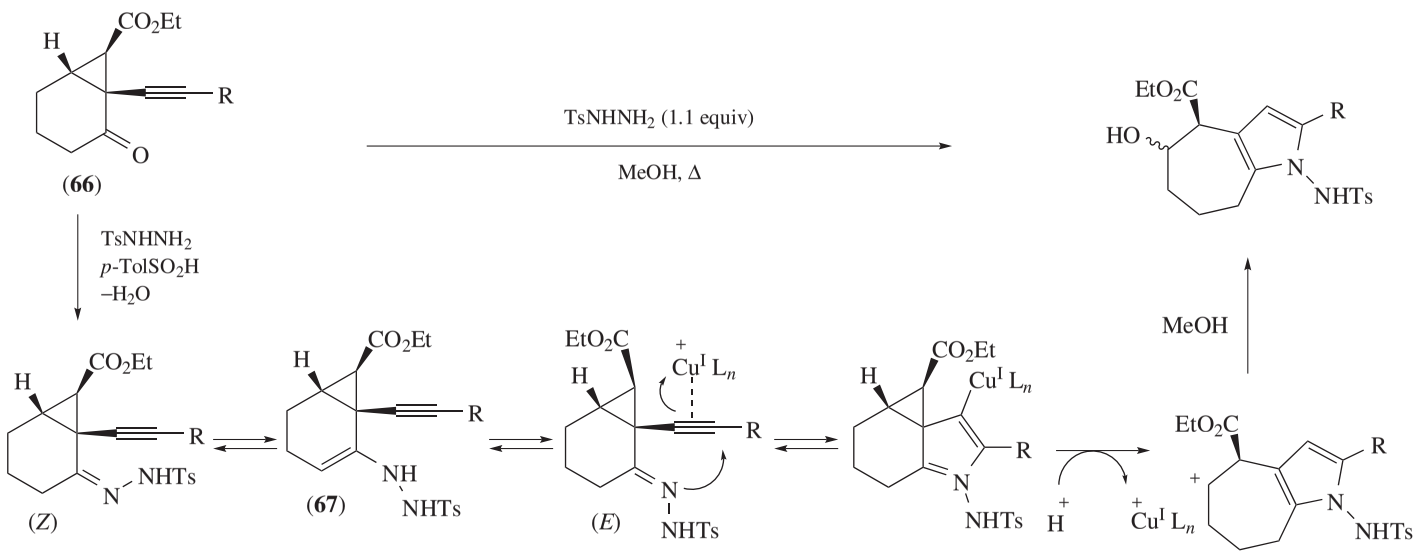
CO2Et
H
R
O
(66)
TsNHNH2 (1.1 equiv)
MeOH, Δ
EtO2C
HO
R
N
NHTs
TsNHNH2
p-TolSO2H
–H2O
MeOH
CO2Et
H
R
NHTs
N
(Z)
(67)
NH
NHTs
EtO2C
Cu^I L_n
(E)
H
+

Scheme 30

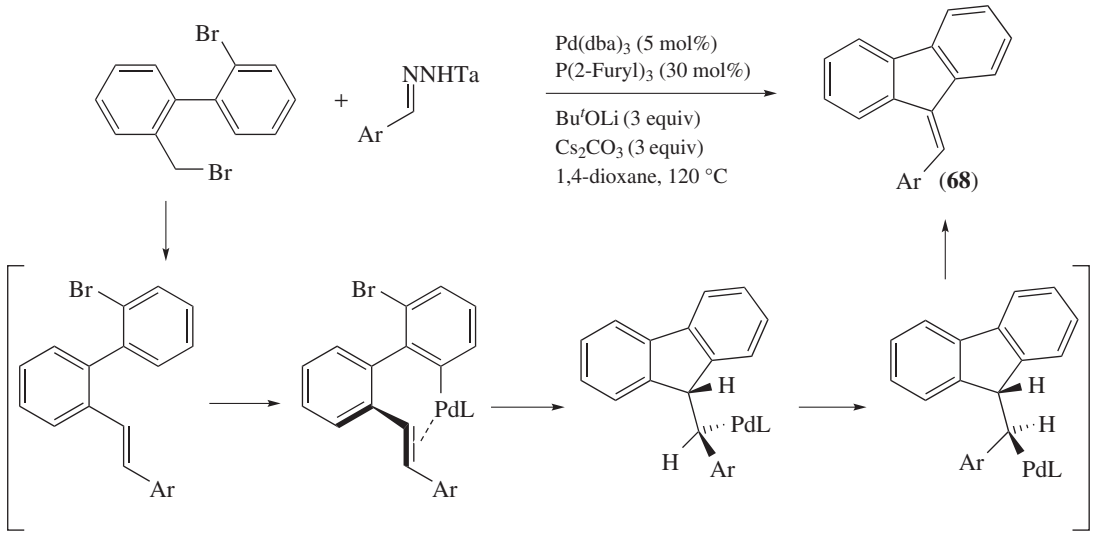

Scheme 31

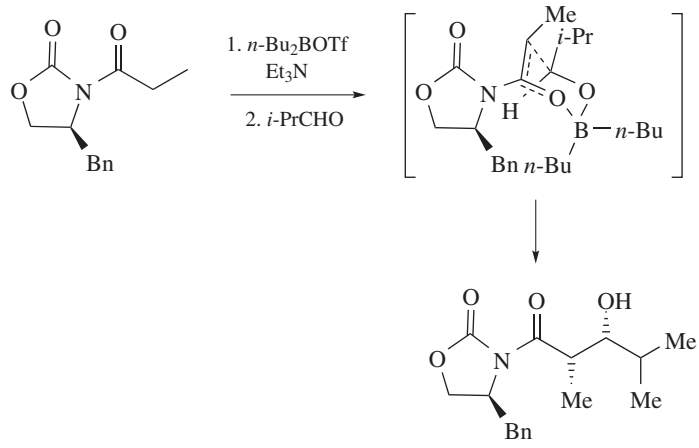

Scheme 32

A metal-free coupling of heteroaromatic *N*-tosylhydrazones with thiols is reported. In the suspected mechanism, the hydrazone is converted into the carbene via the Bamford–Stevens reaction-type reaction mechanism. These carbene couples with thiols to give heteroaryl sulfides.[64] A similar mechanism is proposed in the stannylation of *N*-tosylhydrazones. The alternative pathway, where a diazo compound acts as a nucleophile and no carbene is generated, is unlikely in light of a competition experiment.[65]

C–C Bond Formation and Fission: Aldol and Related Reactions

A combined molecular dynamics and coordinate driving (MD/CD) method for automatically searching multistep reaction pathways for chemical reactions is used to study the intermolecular aldol reaction between vinyl alcohol and formaldehyde. The method was also applied

in the intramolecular Diels–Alder reaction of a ketothioester. For the Diels–Alder reaction, the calculated kinetic product matches the experimental result where the same product was obtained at −78 °C.[66]

Hydroxyapatite (HAp) catalyses the reaction between formaldehyde and glyceraldehyde, producing ribose in one-pot in a low yield. Mechanistic studies suggest that HAp worked continuously for a cross-aldol reaction and Lobry de Bruyn–van Ekenstein transformations by utilizing the effective positioning of columnar calcium ions in the surface of HAp.[67]

Computationally designed biocatalyst RA95 and its evolved variants have different rate-limiting steps in the retro-aldol reaction of methodol. The C–C bond cleavage is the rate-determining step for RA95, while the product release (carbinolamine to acetone) is the slowest step for the evolved enzymes, which are 10^5-fold more active (retro-)aldolase. A complex hydrogen bond network of four active site residues is speculated to enhance lysine reactivity and proton shuffling in the evolved enzymes.[68]

Asymmetric Aldol Reactions

A mechanistic study on the aldol addition of oxazolidinone-derived boron enolates indicates that none of the species along the reaction coordinate show any aggregation. The rate-limiting step is the complexation via a transition structure with a counterion. Hindered amines (the *n*-Bu_2BOTf·*i*-Bu_3N system) shift the rate-determining step to proton transfer. Rate studies show that the aldol reaction with isobutyraldehyde follows the mechanism proposed by Evans in the original work.[69]

The Mukaiyama Aldol

The vinylogous Mukaiyama aldol reaction, using *in situ* generated Lewis acid (**71**), provides access to (**72**) stereoselectively (Scheme 33). The chiral Lewis acid (**71**) is generated from *N*-Ts-L-tryptophan and dichlorophenylborane and co-ordinates with the aldehyde to cause facial discrimination. The TES-ketene acetal attacks from the less-hindered *Re* face, giving preferentially the *R*-configured OH diastereomer.[70] *de*

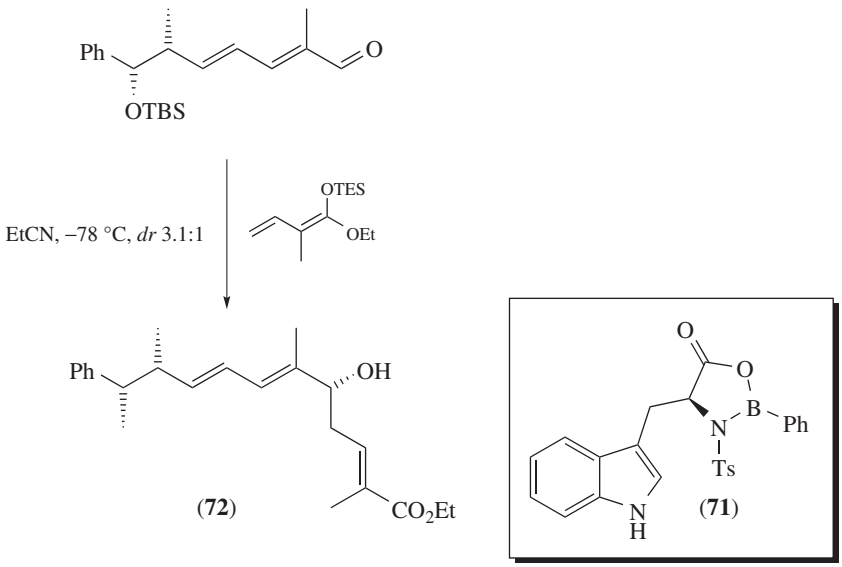

Scheme 33

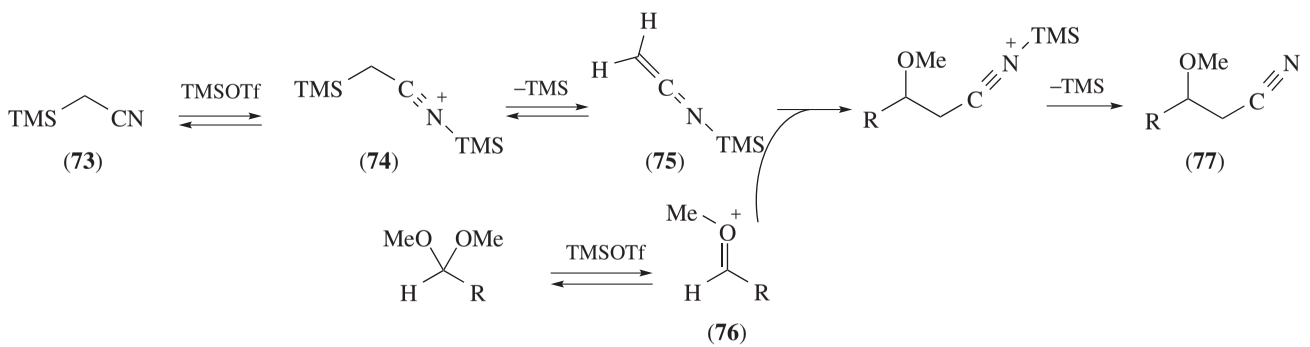

(**73**) (**74**) (**75**) (**77**) (**76**)

Scheme 34

Other Aldol and Aldol-type Reactions

(Trimethylsilyl)acetonitrile (**73**) reacts with dimethyl acetals in the presence of TMSOTf to yield β-methoxynitriles (**5**) (Scheme 34). The proposed mechanism involves activation of (**73**), followed by the desilylation, to give N-silylated ketene (**75**). This reacts with the oxycarbenium ion (**76**), which after silyl transfer provides the product (77). The formation of silylnitrile (**74**) is supported by the observation that the reaction does not provide the product with other Lewis acids or with TfOH.[71]

Oxymercuration followed by aldol cyclization of the pivalate (**78**) gives the tricyclic product (**80**) in much higher yields than the corresponding acetate (**79**) (Scheme 35). The difference in the reactivity of (**78**) versus (**79**) is speculated to be due to subtle differences in the dominant conformation around the C5/C11 axis. The bigger pivaloyl group prefers the conformation (**81**), leading to the desired product, while the smaller acetyl group favours (**82**), which leads to other reaction pathways.[72]

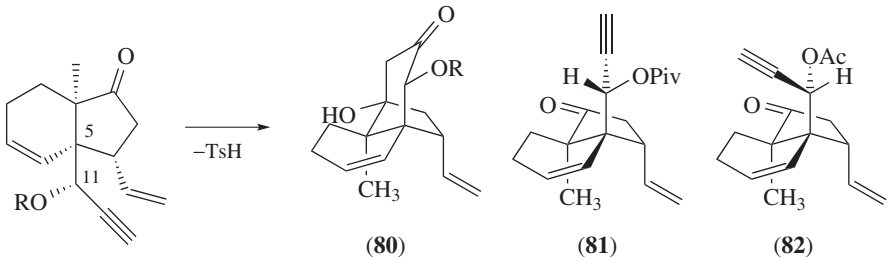

(**78**) R = Piv
(**79**) R = Ac

(**80**) (**81**) (**82**)

Scheme 35

An Ru(II)/iminium-cocatalysed cycloaddition of diazoacetophenones, anilines, and enals provides substituted pyrrolidines in a diastereo- and enantio-selective manner (Scheme 36). The postulated mechanism, supported by the detection of (**83**), involves the selective 1,4-addition of enals, followed by a tandem aza-aldol process. Control experiments and DFT investigations suggest that a reversible NaOAc-facilitated aza-aldol process is responsible for the formation of the thermodynamic diastereomer.[73]

ee
de

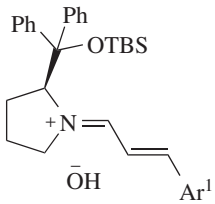

(**83**)

Scheme 36

Reaction of (**84**) with $CuCl_2$ and LiCl in DMF results in an intramolecular aldol condensation, followed by oxidative aromatization, giving (**85**) (Scheme 37). The transformation is speculated to proceed through an α-carbonyl chlorination process, which further undergoes a dehydrochlorination and aromatization, giving (**85**).[74]

An organocatalytic decarboxylative aldol reaction of β-ketoacids with α-ketophosphonates using (**86**) provides tertiary α-hydroxyphosphonates enantioselectively (Scheme 38). A

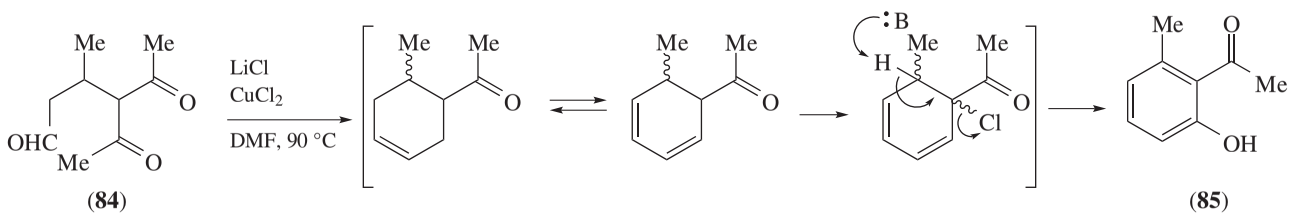

(**84**) (**85**)

Scheme 37

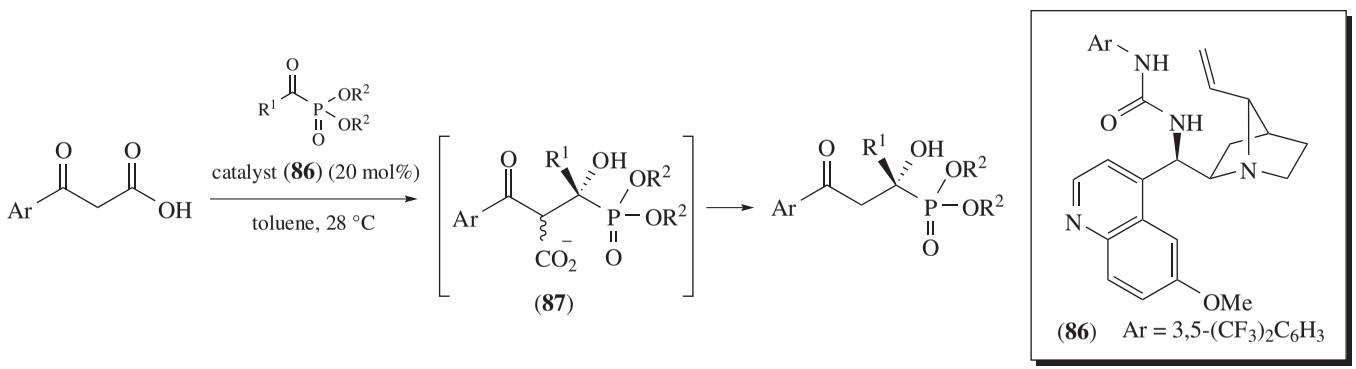

Scheme 38

phosphorus NMR study of the reaction suggests that the reaction goes through the intermediate (**87**).[75] (ee)

Alkynylations

The Ni-catalysed asymmetric reductive coupling reactions of aldehydes and alkynes, performed with an exceptionally hindered NHC ligand (**88**), provide silyl ether in a regio- and enantio-selective manner (Scheme 39). Computational work shows that the regioselectivity is controlled by the substantial steric influence of the ligand, while the enantiocontrol also involves the role that alkyne sterics play in influencing the ligand–aldehyde interactions.[76] (ee)

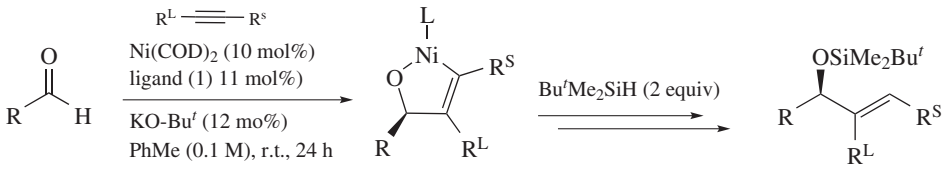

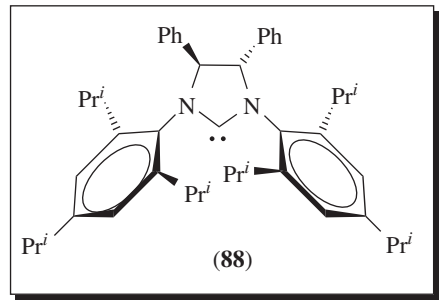

(**88**)

Scheme 39

Michael Addition and Miscellaneous Condensations

A mini review summarizes the recent experimental and theoretical mechanistic studies of catalytic asymmetric 1,4-additions. It also includes models that can be used to predict the outcome of a stereoselective reaction. The review also discusses nonlinear effects and reversal of enantioselectivity, and showcases favoured and disfavoured transition states that help understand the latter phenomenon.[77] (ee)

Kinetic investigations supported by potential energy surface calculations suggest that a single set of electrophilicity parameter *E* for Michael acceptors can be used to calculate rate constants for a variety of reactions which proceed via rate-determining formation of the first C–C sigma bond. The data generated in the study can be used for direct comparison of weak and strong electrophiles. Such comparison is not possible with other methods of relative electrophilicity prediction.[77]

DFT calculations have been used to examine the mechanism and origins of stereoselectivity of cinchona thiourea (**89**)-catalysed asymmetric Michael addition of nitroalkanes to enones (Scheme 40). The transition state originating from pre-reaction complex (**91**) is favoured over others. Other types of pre-reaction complexes that have been proposed earlier are expected to be in rapid equilibrium. However, their relative thermodynamic stabilities do not determine the

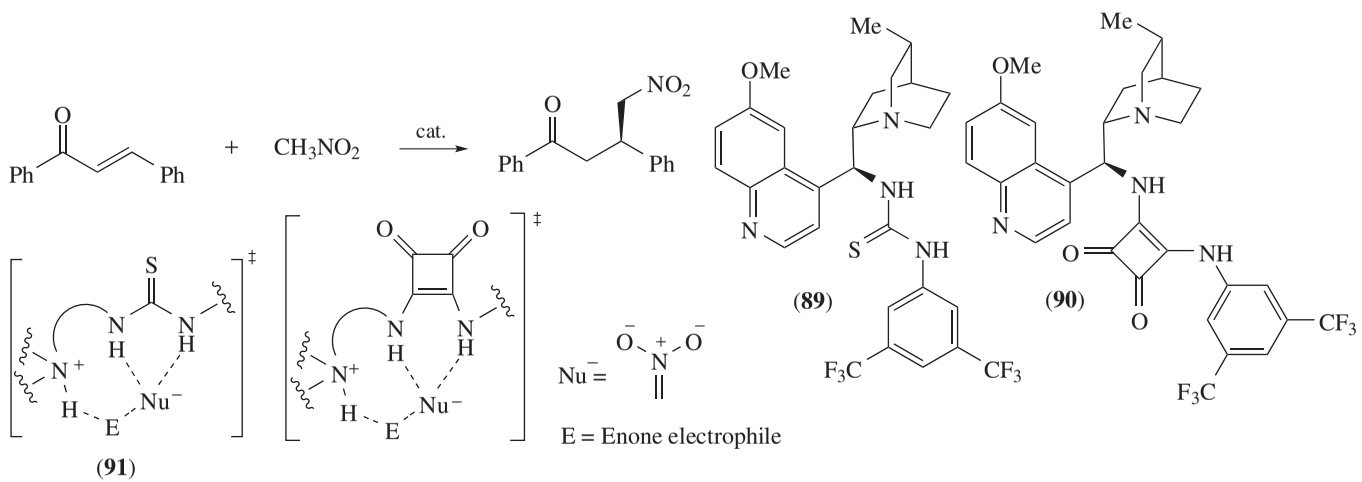
Ph
Ph
+
CH_3NO_2
cat.
NO_2
Ph
Ph
OMe
Me
N
NH
S
NH
F_3C
CF_3
(89)
OMe
Me
N
NH
O
NH
O
CF_3
F_3C
(90)
S
N
H
N
H
N^+
H
E
Nu^-
‡
(91)
O
O
N
H
N
H
N^+
H
E
Nu^-
‡
$Nu^- =$
O^-
N^+
O^-
E = Enone electrophile

Scheme 40

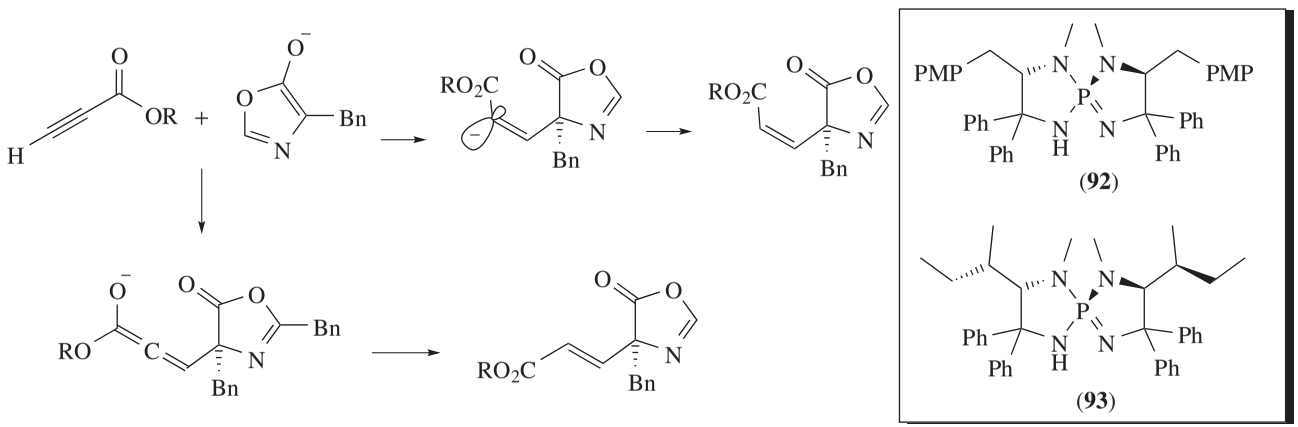

Scheme 41

preferred pathway for the reaction due to Curtin–Hammett conditions. The same mechanism is also operative in the cinchona squaramide (**90**)-catalysed enantioselective sulfa-Michael addition reaction.[78] Stronger noncovalent interactions, namely, hydrogen bond, π-stacking, (ee) and C–H$\cdots\pi$ and C–H$\cdots$F, in the major transition state are the main reason for the observed stereoselectivity.[79]

An ONIOM (QM/MM) study suggests that iminophosphorane-catalysed additions of azalactones proceed via allenyl intermediates with linear (allene-like) or bent (vinyl anion-like) geometries (Scheme 41). There is an innate kinetic preference for the formation of bent *Z*-intermediates in the Michael addition step. Protonation of this intermediate is faster than *Z*/*E* isomerization, leading to *Z*-alkenes (with catalyst **92**). A kinetic preference for the *E*-alkene arises (with catalyst **93**) from the stereoselective α-C protonation proceeding via a linear intermediate.[80]

A domino sequence can convert 2-aminopyridines into 2*H*-pyrido[1,2-*a*]pyrimidin-2-ones. The first Michael addition of 2-aminopyridine on the HFIP-activated (**94**) is proposed to produce the zwitterionic enolate (**95**) (Scheme 42). Calculations (M06-2X-31+G(d,p) + PCM level of theory) suggest that the addition is less endergonic ($\Delta G = +11.55$ kcal mol^{-1}) than the expected attack of primary amine site on (**94**) which can produce (**96**) ($\Delta G = +14.54$ kcal mol^{-1}). Dehydration, followed by acyl substitution, gives the cyclized product (**97**). The pyridopyrimidinone (**97**) undergoes a geometrically disallowed [1,3]-H shift to give the product. Calculations were used to support the [1,3]-H shift as the endergonically favourable step ($\Delta G = -15.77$ kcal mol^{-1}).[81]

A Michael addition/elimination process, followed by a base-induced cyclization, is proposed for the spirocyclization of keto-sulfonamides. The ynamide intermediates are speculated to be formed via a Michael addition/elimination that happens without the need of any metal or a Lewis acid.[82] The reaction of indolin-2-one with (**98**) does not give the expected mono-aza-Michael adduct (Scheme 43). Instead, a double Michael product (**99**) is obtained.[83]

Michael-initiated ring closure (MIRC) of a functionalized cyclopentenone (**100**) with a stabilized sulfonium ylide gives *exo* (CO_2Et outside the cyclopentyl ring) cyclopropyl-cyclopentanes (**101**) and (**102**) (Scheme 44). DFT calculations suggest that selective formation of *exo* products is due to epimerization of unreactive intermediates from the other two pathways. One of the *exo* products (**101**) can be converted completely into a tricyclic product (**105**) in the presence of excess base. Base forms the enolate (**103**), which results in a β-elimination of the ether. The new unsaturated ketone (**104**) undergoes the Johnson–Corey–Chaykovsky cyclopropanation reaction to give (**105**). The same does not occur with (**102**) because of the steric crowding of the cyclopropane ring, which raises the TS energy and destabilizes association of the protonated base.[84]

An organocatalysed [3 + 2] annulation of cyclopropenones and β-ketoesters provides substituted butenolides. Mechanistic studies verify the presence of the enolate intermediate and the involvement of the intermolecular esterification and the intramolecular Michael reaction.[85]

A multi-component reaction involving aldehydes, 1,3-diones, and/or barbituric acid is carried out in the presence of the catalytic amount of L-proline in water at rt, giving several corresponding products in high enantioselectivities (Scheme 45). The proposed mechanism proceeds through the proline-catalysed formation of enedione (**106**). The Michael-type addition of (**107**) on (**106**), followed by cyclization and hydrolysis, gives the product, but no model explaining the enantioselectivities was proposed.[86] (ee)

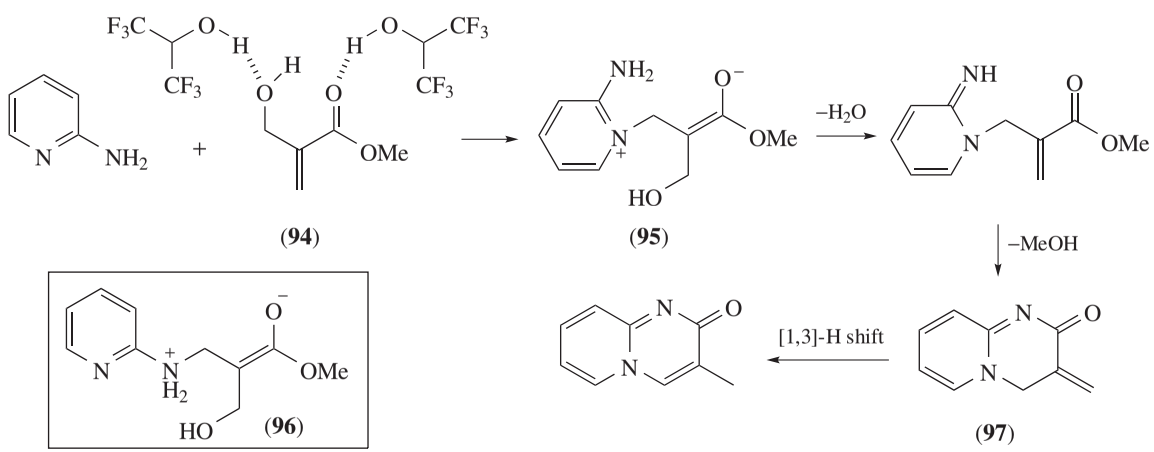
F3C
CF3
O
H
H
O
O
H
O
CF3
CF3
N
NH2
+
OMe
(94)
NH2
O−
N+
OMe
HO
(95)
−H2O
NH
O
N
OMe
−MeOH
N
O
N
[1,3]-H shift
N
O
N
(97)
O−
N
N+
H2
OMe
HO
(96)

Scheme 42

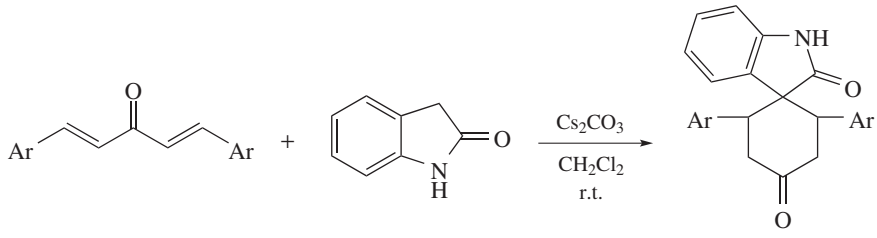

(**98**) (**99**)

Scheme 43

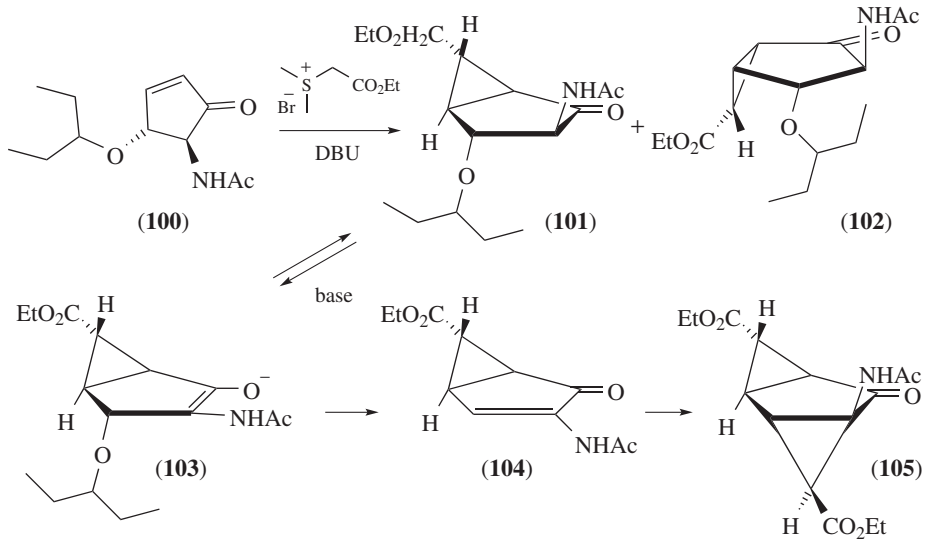

(**100**) (**101**) (**102**) (**103**) (**104**) (**105**)

Scheme 44

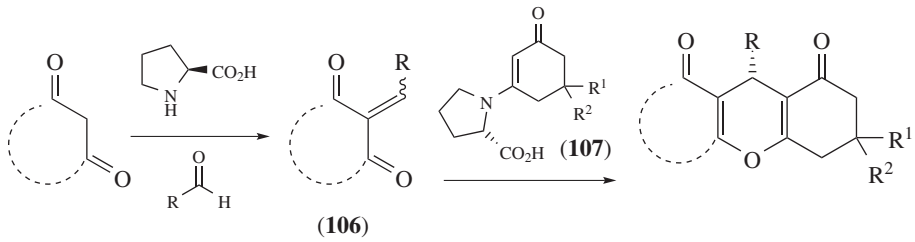

(**106**)

Scheme 45

A novel series of substituted pyrazolo[3,4-*b*]pyridines (**111**) has been reported by the microwave-assisted condensation of (**108**) and (**109**) (Scheme 46). The proposed mechanism involves a Michael-type addition of (**108**) on (**109**), followed by an intramolecular ring opening to form intermediate (**110**). Intramolecular attack of the pyrazole carbon to a carbonyl group leads to dihydropyridine. Dehydration of this species provides (**111**). The mechanism successfully accounts for formation of by-products (**112**) and (**113**). These can arise as a result of the hydrolysis of (**109**) under the reaction conditions. Intermediate (**110**) is obtained when the reaction was run at a lower temperature. Isolated (**110**) can be converted into (**111**) under the optimized reaction conditions for the direct formation of (**111**).[87]

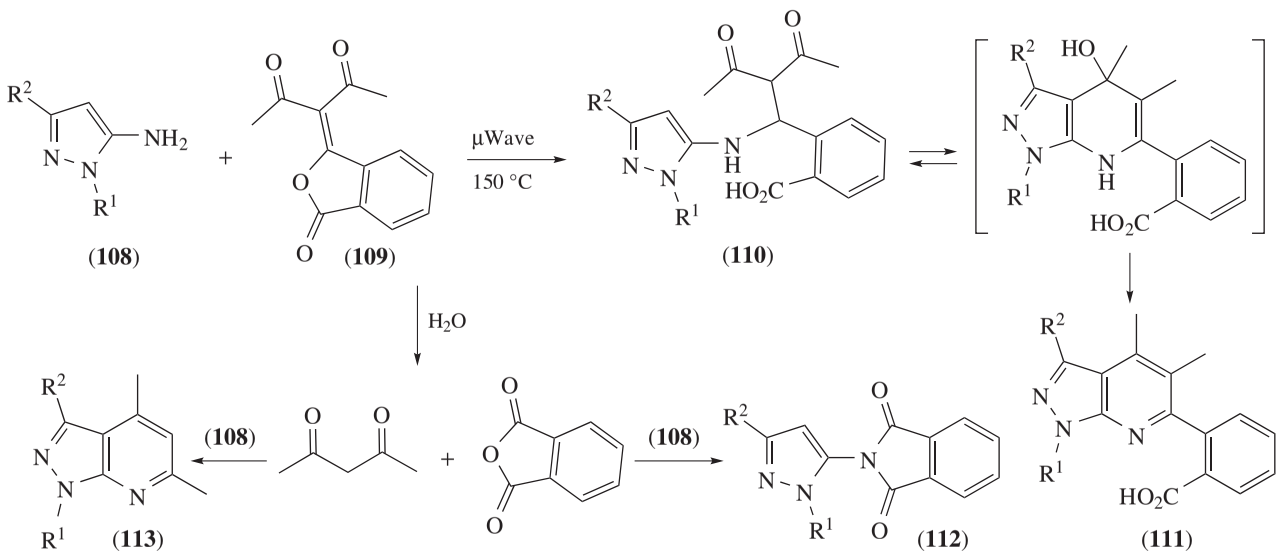

Scheme 46

An azetidine-driven dinuclear zinc performs the asymmetric phospha-Michael addition of diallyl phosphite to α,β-unsaturated carbonyl compounds. A nonlinear effect is identified by measuring the correlation of the *ee* between the product and the chiral ligand. It is speculated that the active catalyst species is Zn_2EtL (L = ligand).[88]

An *N*-heterocyclic carbene catalyses the glycosylation of 2-nitrogalactals with alcohols and phenols. The products show α-selectivity. Experiments indicate that the C-4 stereocentre on the galactal is responsible for the stereocontrol. The NHC–HOR complex is proposed to be involved in the reaction and the Michael addition of the hydroxyl group to the 2-nitrogalactal from the sterically favoured side.[89]

Disubstituted γ-pyrones are prepared from β-ketoacids with the help of Tf_2O. Decreasing the electron density on the aromatic ring in the starting materials gives lower yields of the corresponding products. Such β-ketoacids, with decreased electron density, could undergo a decarboxylation prior to the condensation more readily, thus giving decreased overall yields of γ-pyrones.[90]

The *trans*/*cis* ratio of the amide bond is a key factor in the enantio- and diastereo-selectivity of peptide catalysts in conjugate additions. Catalyst analogues with different ring sizes produce different *trans*/*cis* ratios in different solvents and show a linear correlation between the amount of *trans* conformer of the peptide catalyst and their enantioselectivities. The *trans* conformer is a more selective catalyst than the *cis* conformer.[91]

ee
de

Kinetic analysis reveals a reaction order of 1 in iodine, in iodine-catalysed Michael additions, ruling out the possibility of the involvement of higher iodine species in the rate-limiting step. Experimental investigations rule out the possibility of HI catalysis by partial decomposition of I_2. Instead, a halogen bond activation mode is solely responsible for iodine catalysis. Compared with typical Lewis acids, iodine catalysis is superior in Michael additions.[92]

A new variant of Feist–Bénary reaction (IFB) has been reported. In this three-component 'interrupted' IFB reaction, 1,3-dicarbonyl compounds react with isatin and *N*-phenacyl pyridinium salts to give spirooxindole-furan derivatives (Scheme 47). The reaction is proposed to go through the Knoevenagel reaction between isatin derivatives and 1,3-dicarbonyl compounds giving adducts (**114**). Deprotonation of a pyridinium salt gives a pyridinium ylide (**115**). The Michael addition of the pyridinium ylide (**115**) on the Knoevenagel adduct (**114**), followed by cyclization, provides the spirooxindole-furan derivatives (**116**).[93]

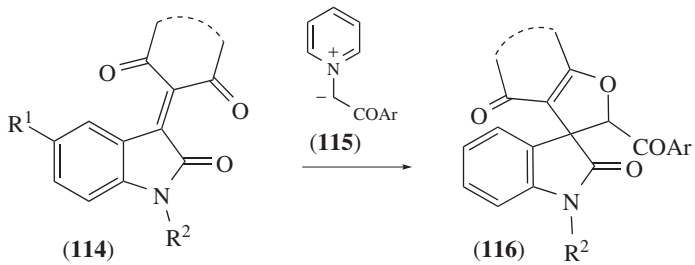

Scheme 47

Other Addition Reactions

An acid-catalysed chemoselective reaction between substituted 2-aminothiazoles and aldehydes produces bis(thiazole-2-imine)methanes (Scheme 48). The chemoselectivity is attributed to be a result of the in-plane position of the primary amine group, which reduces its nucleophilicity due to tautomerization. The ring nitrogen of the tautomeric form is more nucleophilic and reacts with aldehydes to form intermediate (**117**), thus leading to the product.[94]

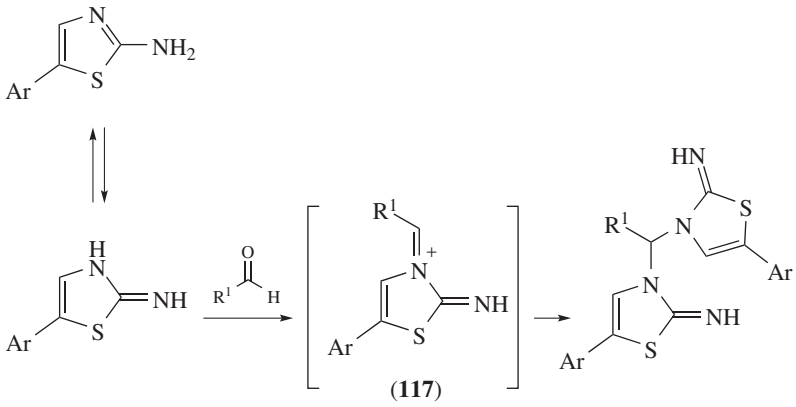

Scheme 48

Prolinate salts catalyse the α-aminoxylation reaction of aldehyde and nitrobenzene. A reaction model is proposed on the basis of NMR studies, solubility data, and by performing a reaction in the presence of molecular sieves. The results show that water, generated in the enamine formation, is essential in this reaction. It protonates the nitrogen of nitrosobenzene and forms a hydrogen bond with the carboxylate. The study also provides support in favour of the Houk–List model of proline-mediated reactions.[95]

An acetyl chloride-mediated reaction of ethyl glyoxylate, primary carbamates, and various types of nucleophiles gives protected α-aminoesters. The halogenation step is identified as the rate-determining step toward the formation of α-chloroglycine. The kinetic studies of the nucleophilic substitution support an S_N1-like (S_N2C+) mechanism involving the nucleophilic attack to the iminium–chloride tight ionic pair.[96]

Arylations

A metallaphotoredox reaction enables C–H arylation and alkylation of aldehydes. The proposed mechanism involves three catalytic cycles balanced by oxidation and reduction potentials of various species. The quinuclidinium radical cation enables kinetic selectivity, and the quinuclidine catalyst is regenerated via deprotonation of the quinuclidinium ion with K_2CO_3.[97]

Addition of Other Organometallics, including Grignards

Reaction of silyllithium, α-keto *N-tert*-butanesulfinyl imidates, and aldehydes gives α,β-dihydroxy acid derivatives in a diastereoselective manner. The stereochemical outcome is rationalized via the transition state in which the (*E*)-aza-enolate approaches the aldehyde from the *Re* face. This orientation is favourable due to less interactions between *R* and the silyoxy group and *R* and the *N*,*O*-acetal group. Furthermore, the *tert*-butyl group blocks one face of the enolate.[98] (de)

The Wittig, Julia-Kocienski, Peterson, and Other Olefinations

A survey of carbonyl-stabilized phosphonium ylides shows that thermal extrusion of PPh_3O for the formation of alkynes is not possible for cases where $^2J_{P-CO}$ is greater than 11 Hz. ^{13}C NMR can be used to measure these *J* values.[99]

Tetrasubstituted fluoroalkenes can be synthesized with high *E*/*Z* selectivity by the Wittig reaction between α-heterosubstituted ketones and α-fluorophosphonium ylides. Calculations

suggest that the observed stereoselectivity is due to stabilizing CH· · ·F and N· · ·C=O interactions in the oxophosphetane TS leading to the *E* isomer.[100]

The Wittig reaction can be performed using the phase-transfer medium (aq. $NaOH/CH_2Cl_2$ 1:1 or $Bu^tOK/Bu^tOH/CH_2Cl_2$ 1:1). Wittig olefination reaction that fails due to poor solubility of phosphonium salts under conventional conditions gives high yields of products using the phase-transfer medium.[101]

The Wittig reaction of (**118**) with aromatic and aliphatic aldehydes gives mono- and bis-alkenyl substituted products. The monosubstituted products are speculated to form due to the regioselective reaction of (**118**) with H_2O.[102] The reaction between Ph_3PCCO and (**119**) does not provide (**120**), but instead gives (**121**) when the reaction is refluxed in toluene (Scheme 49). Formation of the product is explained as a result of stabilized phosphorus ylide formation, which undergoes Wittig olefination to give (**120**). Under the reaction conditions, (**120**) undergoes an intramolecular Michael reaction, producing (**121**). Compound (**120**) can be obtained, without (**121**), if the reaction is run in a sealed tube at 70 °C.[103]

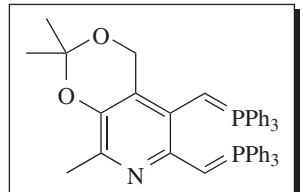

(**118**)

Dimethyl sulfoxide provides a one-carbon source in a transition-metal-free methylenation of ketones (Scheme 50). A thioether intermediate is detected and converted to the enone under the reaction conditions. On the basis of these and other mechanistic experiments and literature reports, it is speculated that DMSO is activated by $K_2S_2O_8$ to give (**122**), which couples with (**123**), producing the intermediate which on subsequent elimination affords the product.[104]

The Wittig reaction of biotinylated phosphorene ylide with peptides exhibits reaction rates of 0.07–5 M^{-1} s^{-1} in water at pH 6.5–8. The low *E*/*Z* selectivity in these reactions is speculated to be due to incomplete cancellation of dipole–dipole interactions in any conformation in the transition states leading toward oxaphosphetanes. The Michael reaction on the product enones occurs with $k = 0.12$ M^{-1} s^{-1} at pH 7.8.[105]

The Borata–Wittig reaction of non-enolizable aldehydes and ketones provides the corresponding alkenes. The reaction proceeds via the formation of lithio oxaboretanide, which was isolated and characterized. The starting lithio-borata-alkene can be generated *in situ* from alkenes via hydroboration followed by deprotonation.[106]

2-Fluoroethoxyphosponates are employed in the Horner–Wadsworth–Emmons (HWE) reaction to ensure high *E*-selectivities when using electron-rich heterocycles (Scheme 51). The epimerization of (**124**), prior to the formation of oxaphosphetane, is proposed. Such epimerization does not happen in the non-fluorinated counterpart of (**124**). However, the possibility of a retro-HWE reaction, promoting the thermodynamically favourable formation of *E*-olefin, cannot be excluded.[107]

Chiral calcium phosphate catalyses the alkenylation of arylglyoxals with 3-vinylindoles. The catalyst activates the hydrate which becomes chiral after this coordination and thus controls the stereoselectivity. ^1H NMR studies were performed to support the mechanistic proposal.[108]

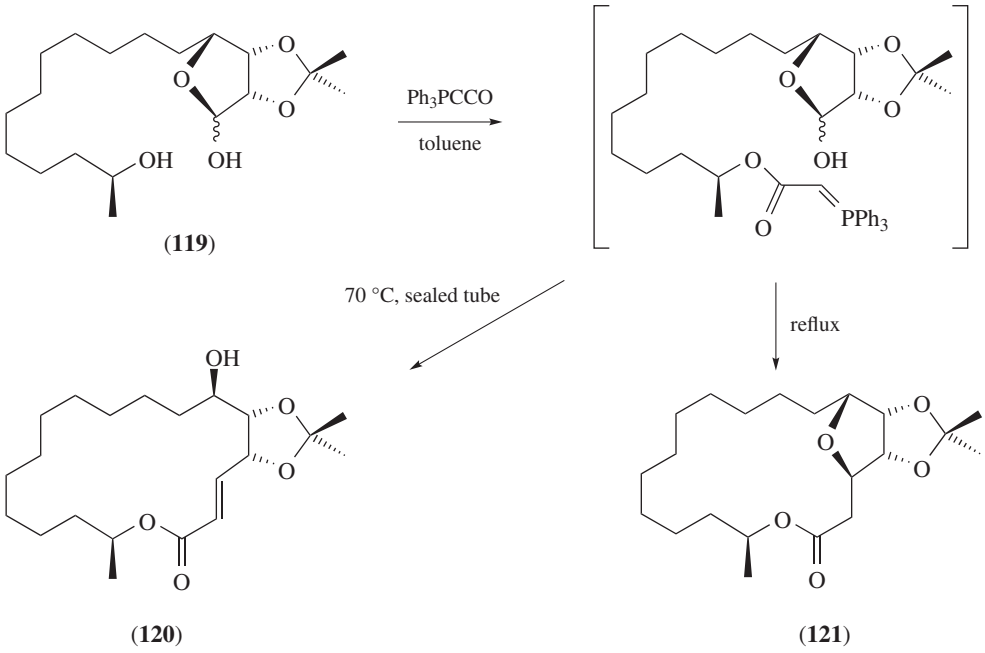

(**119**)

(**120**)

(**121**)

Scheme 49

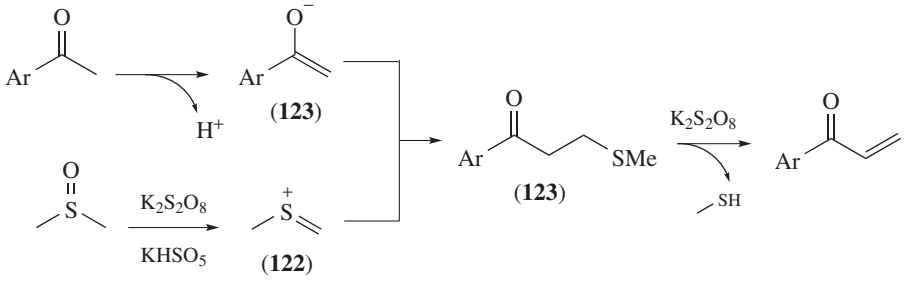

Scheme 50

Hydrophosphonylation, Hydroboration, and Addition of Isocyanide

Choline hydroxide (ChOH) acts as a basic ionic liquid catalyst in the hydrophosphonylation of aldehydes. In the proposed mechanism, the aldehyde is activated via hydrogen bonding with ChOH, which in turn influences the phosphite–phosphonate equilibrium. After hydrogen-bond formation, the phosphite attacks the carbonyl carbon, giving the α-hydroxyphosphonate.[109]

Miscellaneous Additions

Lanthanide amide-catalysed functionalization of isatin (**125**) provides (**126**) and (**127**) (Scheme 52). A mechanism involving the anion of (**128**) is proposed, which is supported by the isolation of (**128**).[110]

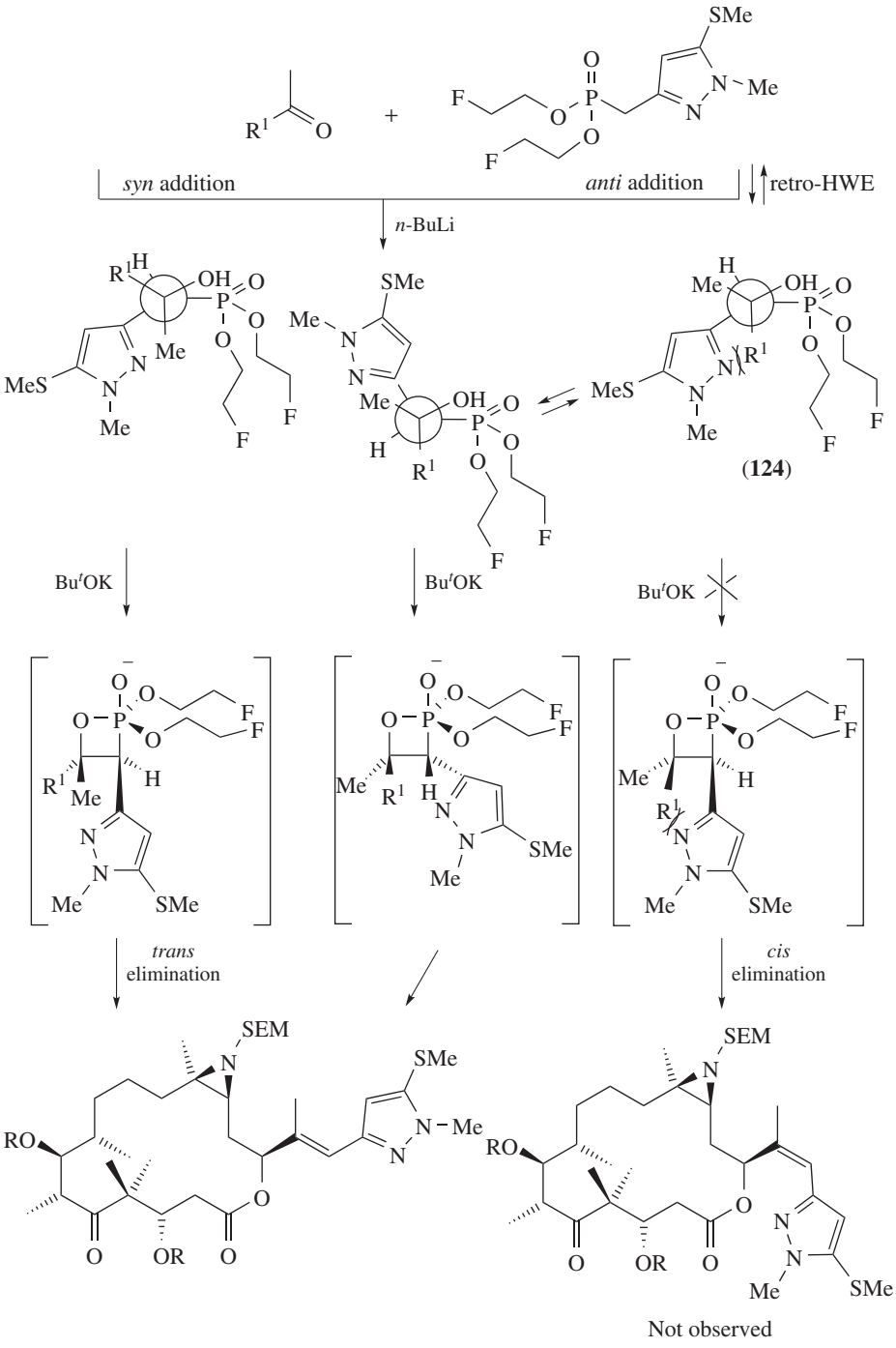
SMe
R1
O
+
F
O
P
O
N
Me
N
F
syn addition
anti addition
retro-HWE
n-BuLi
R1
H
OH
O
P
O
O
MeS
N
N
Me
F
Me
SMe
H
(124)
ButOK
ButOK
ButOK
trans
elimination
cis
elimination
SEM
RO
OR
Not observed

Scheme 51

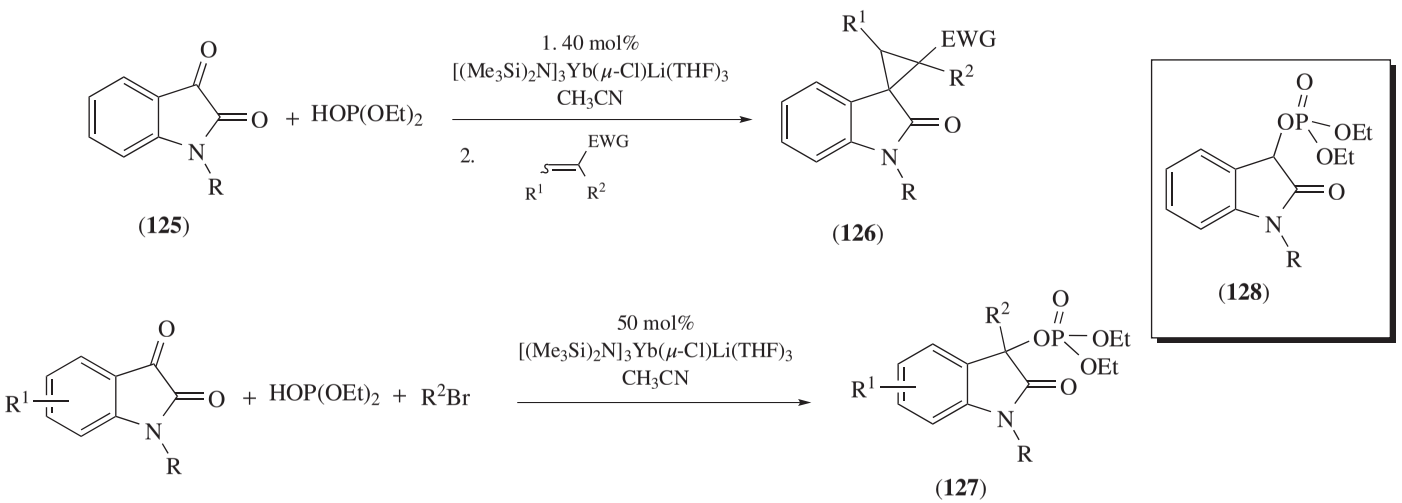
1. 40 mol%
[(Me3Si)2N]3Yb(μ-Cl)Li(THF)3
CH3CN
2.
EWG
HOP(OEt)2
(125)
(126)
(128)
50 mol%
[(Me3Si)2N]3Yb(μ-Cl)Li(THF)3
CH3CN
HOP(OEt)2 + R2Br
(127)

Scheme 52

N-Heterocyclic carbenes catalyse the silyl-Reformatsky reaction of aldehydes with difluoro(trimethylsilyl) acetates. A mechanism involving the NHC attack on the silicon atom is proposed (Scheme 53). The resulting hexavalent species (**129**) initiates the addition with aldehyde, producing intermediate (**130**). The oxy anion of (**130**) attacks the TMS group to form the silyl ether, which after acidic workup affords the *gem*-difluoro ester alcohol.[111]

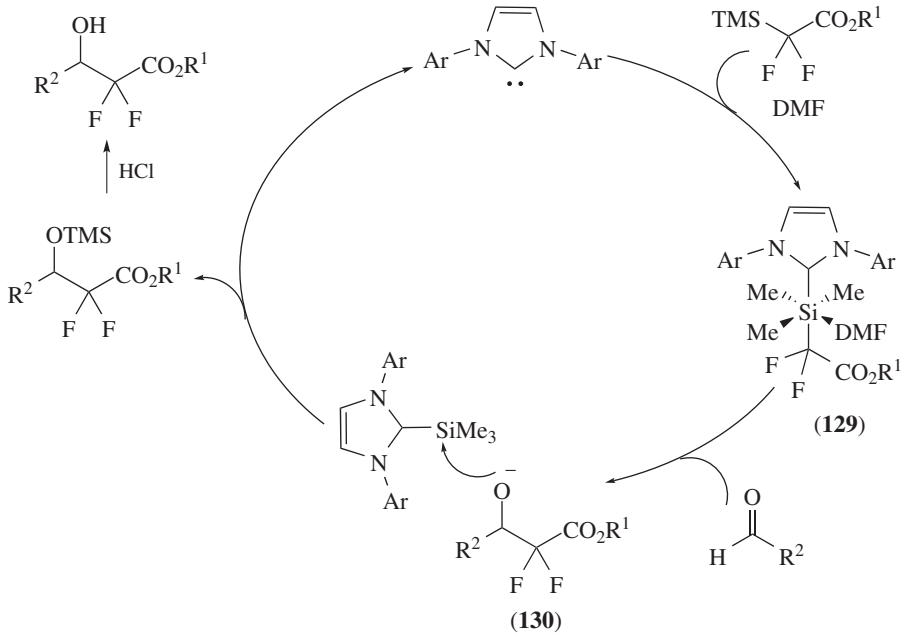

Scheme 53

Flavonoids are synthesized by a Pd-catalysed intramolecular acylation of alkenyl bromides and aldehydes. Two competitive catalytic cycles are proposed. Both processes start with the initial oxidative addition of alkenyl bromide. Cycle A goes through carbopalladation and β-hydride elimination, while cycle B undergoes a C–H activation, loss of HX from the resulting Pd(IV) intermediate, and reductive elimination.[112]

Pyridine-boryl radicals provide C-4-substituted pyridine derivatives via a radical addition/coupling mechanism (Scheme 54). Computational and experimental studies suggest that the pyridine-boryl radical (**131**) is in equilibrium with its dimer, with the equilibrium constant favouring (**131**). The addition of (**131**) to enone may be 1,2 or 1,4, and the two pathways are under an equilibrium, with the 1,4-product being thermodynamically more stable. The pyridine-boryl radical (**131**) is capable of adding to aldehydes, ketones, aryl imines, and alkynones.[113]

The regioselectivity of phosphite addition to $\alpha,\beta,\gamma,\delta$-unsaturated imines can be controlled by the stoichiometry of reagents to provide mono-1,2-addition products (Scheme 55). However, both steric and electronic properties of the substrate differentiate between 1,6- and 1,4-addition. Experimental and theoretical calculations suggest that the mono-1,2-addition of phosphite provides the kinetic product. However, it is also the most reversible type of addition product. In the presence of excess acid, the 1,2-addition can be rendered irreversible. Compound (**132**) undergoes an intermolecular TMS shift and protonation process, which after workup gives the phosphonate. In the presence of excess phosphite, the product distribution is dictated by the thermodynamic stability of the final 1,6- or 1,4-phosphite addition products.[114]

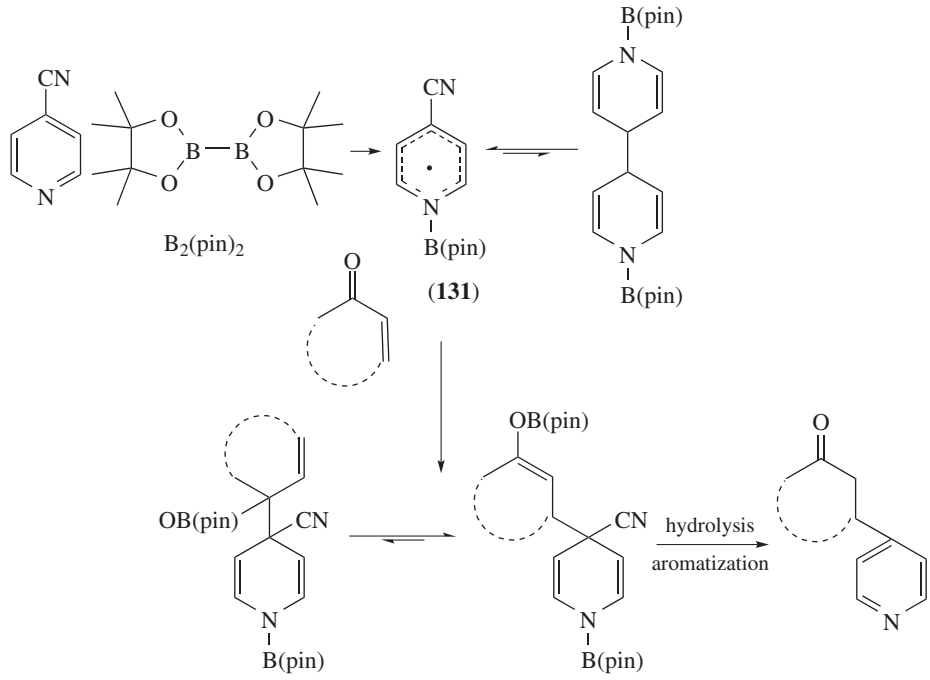

Scheme 54

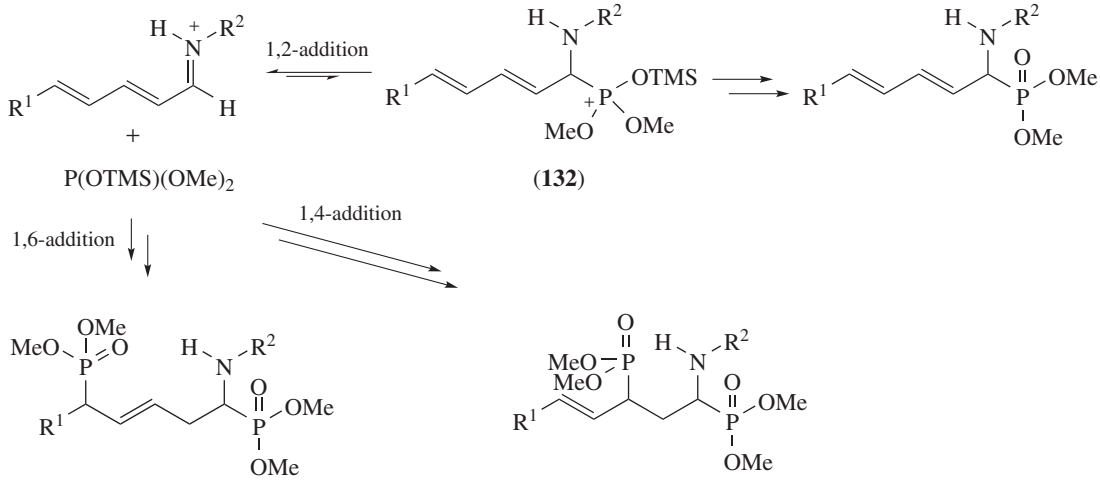

Scheme 55

Enolization, Reactions of Enolates, and Related Reactions

α-Substitutions

Aromatic ketones, in the presence of KSeCN and *tert*-butyl hydroperoxide (TBHP) and KOAc, provide α-carbonyl selenocyanates (Scheme 56). Addition of BHT inhibits the reaction. A small quantity of (**133**) can be isolated in some of these reactions. Compound (**133**) reacts with KSeCN under the above reaction conditions, providing α-carbonyl selenocyanates, via a radical

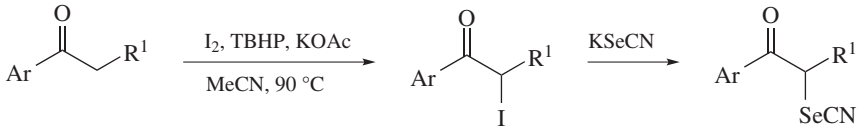

(**133**)

Scheme 56

mechanism.[115] The function of KOAc is probably to neutralize any acid that may be generated in the reaction.

A review was published that describes recent synthetic approaches to *N*,*N*-dimethyl-*β*-keto-enamines. The review mainly describes the use of *N*,*N*-dimethylformamide dimethyl acetal (DMF–DMA) as an efficient *β*-(dimethylamino)methylenating agent for the preparation of enaminones. A few proposed mechanisms, where enaminones are converted into heterocycles, have been mentioned.[116]

Theoretical kinetic studies on the multichannel thermal decomposition of acetaldehyde show that isomerization of CH_3CHO to the enol-form CH_2CHOH is the dominant decomposition pathway at high pressures and low temperatures. At high temperatures, decomposition to CH_3 and CHO becomes dominant.[117]

Oxidation and Reduction of Carbonyl Compounds

Oxidation of Aldehydes to Amides and Nitriles

Aldehydes are converted into nitriles with NH_2OH and then CuO in acetonitrile. The proposed pathway takes into account experimental observations that the reaction does not proceed in EtOH, and the by-product of the reaction is acetamide.[118]

Decarbonylation Reactions

Aromatic aldehydes undergo a decarbonylation reaction with Ni(0) when heated at 140 °C in a sealed tube (Scheme 57). The Tishchenko reaction is a competing reaction, although this is suppressed when *ortho*-substituted aldehydes are used. Both steric and electronic factors are hypothesized as being responsible for this effect. During the mechanistic study, complex (**134**) was isolated, which does give a decarbonylated product upon heating, suggesting the possibility that it is an intermediate.[119]

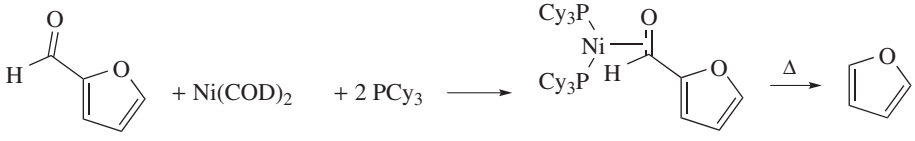

(**134**)

Scheme 57

A Pd(II)-catalysed decarboxylative acylation of aromatic ketones with *α*-oxocarboxylic acids gives 1,2-diacylbenzenes (Scheme 58). A mechanism involving the reaction of palladacycle (**137**) with acyl radicals is suggested, and this is supported by the fact that (**137**) is kinetically competent for catalysing the reaction between (**135**) and (**136**). The KIEs, the Hammett constants, and the isolation of the (**137**) and TEMPO adduct also support the proposed mechanism.[120]

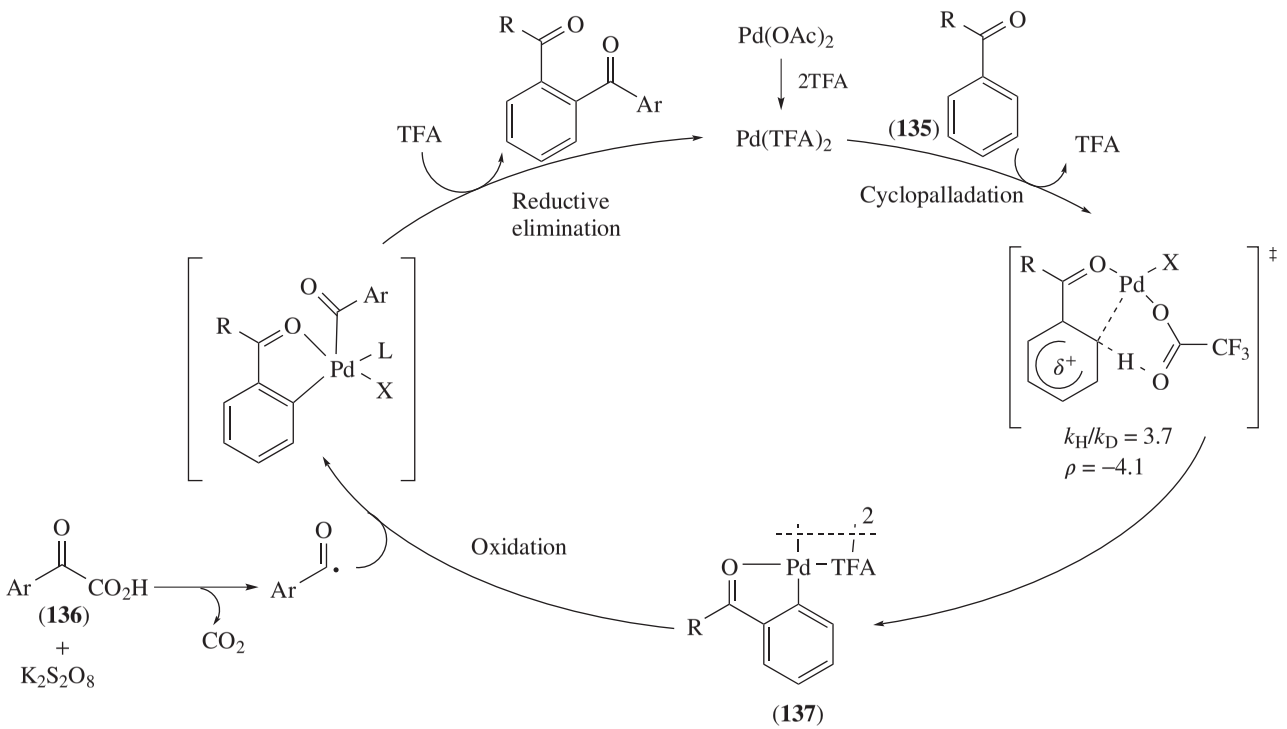
Pd(OAc)2
2TFA
Pd(TFA)2
(135)
TFA
Cyclopalladation
Reductive elimination
TFA
kH/kD = 3.7
ρ = –4.1
Oxidation
(136)
+
K2S2O8
CO2
(137)

Scheme 58

The nickel/NHC-mediated decarbonylation of ketones has been reported (Scheme 59). Competition experiments and IR studies suggest an initial non-reversible oxidation of Ni across one of the C(aryl)–C(=O) bonds. The resulting species undergoes a decarbonylation reaction to give (**138**). Reductive elimination of (**138**) results in the formation of the biaryl product.[121]

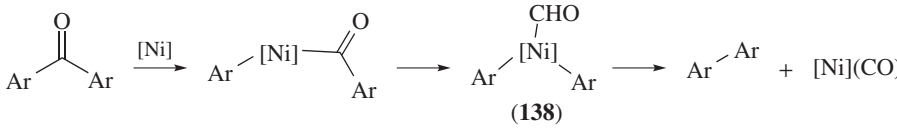

Scheme 59

Enantioselective decarboxylative α-alkynylation of β-ketocarbonyls provides corresponding adducts via a catalytic α-imino radical intermediate (Scheme 60). Stern–Volmer fluorescence quenching studies suggest that (**139**), formed *in situ* from the corresponding acid, serves as the precursor of BI radical. The radical is quenched by photoexcited $[Ru(bpy)_3]^{2+*}$ to Ru(III), which then oxidizes the enamine intermediate which loses a proton to give the α-imino radical intermediate (**140**). A TS involving H bonding with (**139**) is proposed to rationalize enantioselectivity.[122]

Miscellaneous Oxidative Processes

The formation, oxidation, and fate of the Breslow intermediate are reported in the *N*-heterocyclic carbene-catalysed aerobic oxidation of aldehydes. This is the first report where the Breslow intermediate is observed and characterized in the gas phase. Computational studies, utilizing the nudged elastic band procedure, show that the detection of the Breslow intermediate is possible because of the limited reactivity of the Breslow intermediate when it has the *ortho*-bromo-substituted aromatic ring.[123]

The direct N-acylation reaction of primary amides with aryl/α,β-unsaturated aldehydes is possible by an NHC-catalysed process in the presence of an inorganic base and 3,3′,5,5′-tetra-*tert*-butyldiphenoquinone (DPQ) (Scheme 61). The proposed catalytic cycle involves formation of the Breslow intermediate (**141**) and its oxidation. Nucleophilic attack of the deprotonated amide on this intermediate and regeneration of the catalyst via elimination complete the cycle.[124]

The C–C coupling of acetone at α-position can be achieved using the H_2O/UV light system. In the proposed mechanism, the UV irradiation of H_2O_2 provides OH radicals, which cleave the α-CH of acetone. The intermediate then undergoes C–C coupling to yield 2,5-hexandione. The selectivity of the reaction can be enhanced by controlling the OH radical concentration.[125]

The high-level theoretical study on the reactions of methacrolein (MACR) and methyl vinyl ketone (MVK) with a hydroperoxyl radical shows that the most favourable pathway is the concerted addition of the terminal O of HO_2 radical to the carbonyl carbon and H-transfer from HO_2 radical to the carbonyl oxygen, forming the α-hydroxyalkenylperoxy radical. The rate of this reaction decreases as the temperature increases from 200 to 500 K.[126]

Alcohols and aldehydes can be converted into 1*H*-tetrazoles when reacted with NaN_3 and NH_3 in the presence of catalytic amounts of $Cu(NO_3)_2$ (Scheme 62). The reaction is suspected to involve the formation of an imine, its oxidation to a nitrile, formation of intermediate (**142**) via activation of the nitrile, and its subsequent 1,5-cyclization. Transmetallation with NaN_3, followed by protonation during the acidic workup, then provides tetrazoles.[127]

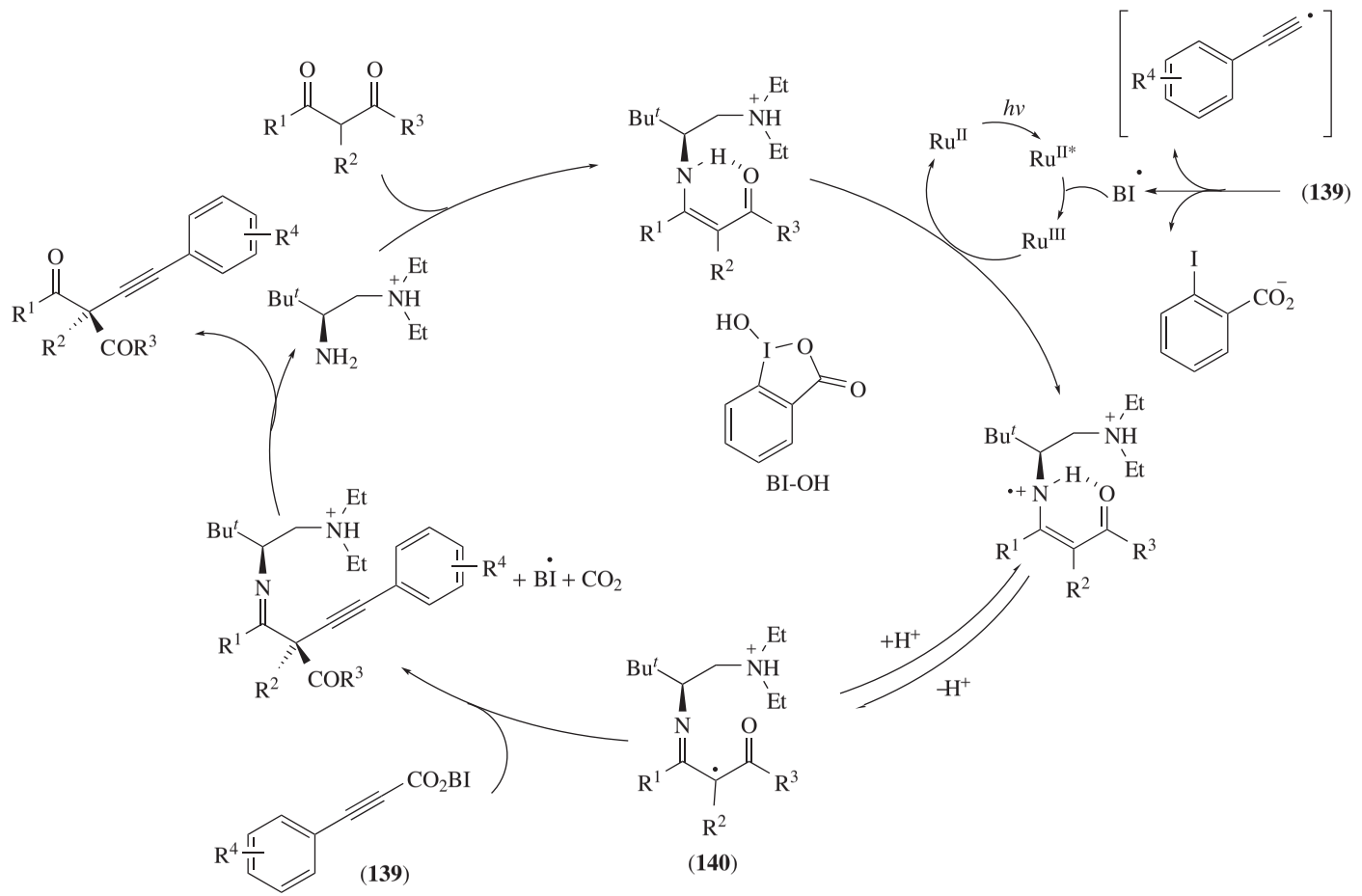

Scheme 60

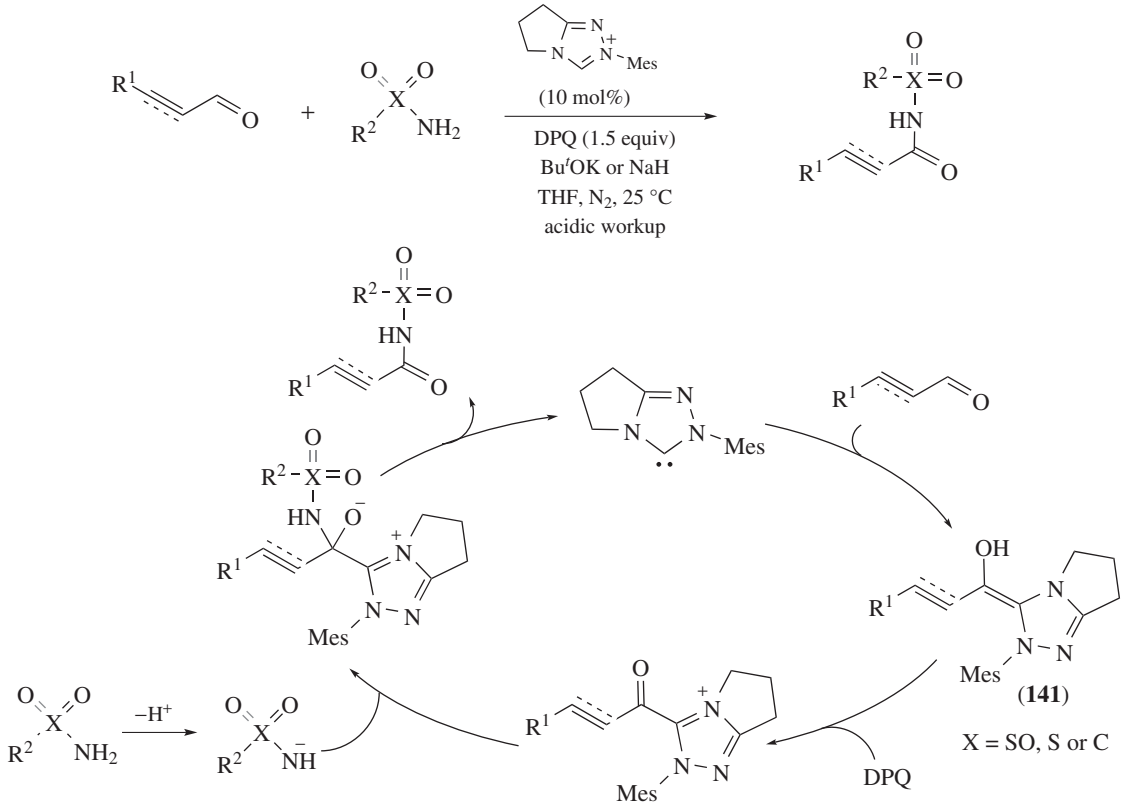

Scheme 61

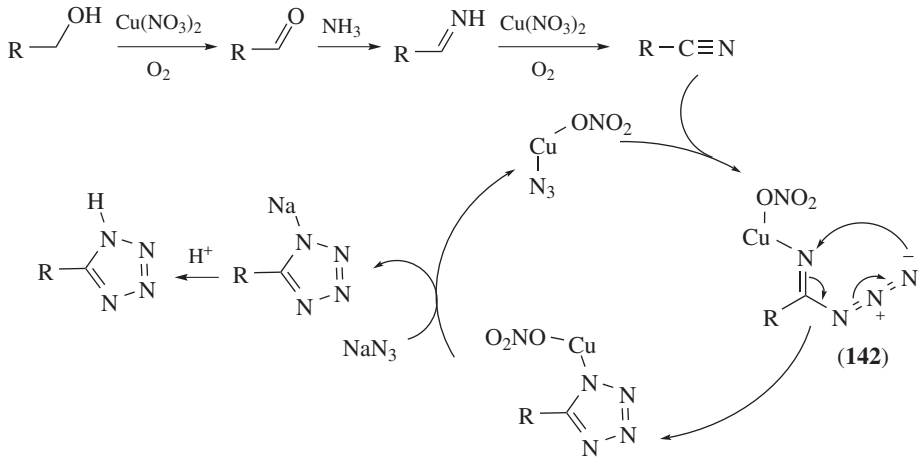

Scheme 62

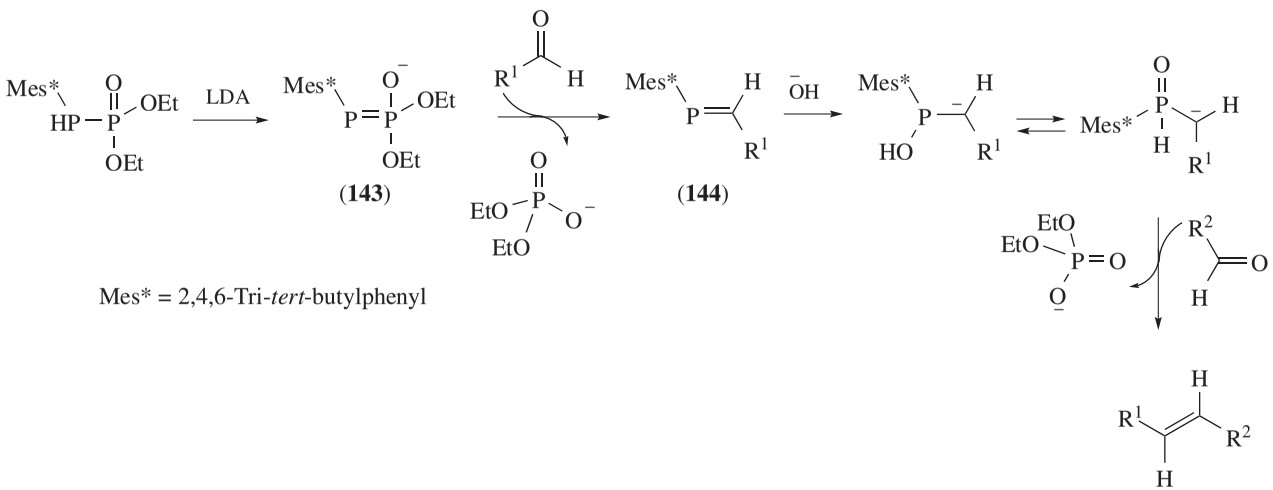

Mes* = 2,4,6-Tri-*tert*-butylphenyl

Scheme 63

Stereoselective Reduction Reactions

The intermolecular reductive coupling of two different aldehydes affords *E*-alkenes (Scheme 63). First, the aldehyde reacts with (**143**) affording phosphaalkene intermediate (**144**). Intermediate (**144**), upon activation by hydroxide, reacts with a second aldehyde giving unsymmetrical *E*-alkenes. The proposed mechanism is supported by ^{31}P NMR spectroscopic studies of the individual steps.[128]

An Sm(II)-induced ring-expansion reaction provides methylenebicyclo[3.2.1]octanols (Scheme 64). A mechanism is suggested in light of an isotope labelling experiment and the identification of the OH derivative of intermediate (**145**). The mechanism involves generation of a ketyl radical by single-electron reduction with Sm(II), ketyl-olefin cyclization, fragmentation of (**145**), and the reduction of the resulting radical by Sm(II). Protonation of this species finally renders (**146**).[129] The reaction involves adding LiCl to the reaction mixture containing SmI_2. This generates $SmCl_2$ *in situ*; the latter is a stronger reducing agent. One electron transfer, leading to (**145**), most likely from $SmCl_2$, happens through the inner-sphere mechanism (Takatori, K., Personal Communication, April 25, 2019).

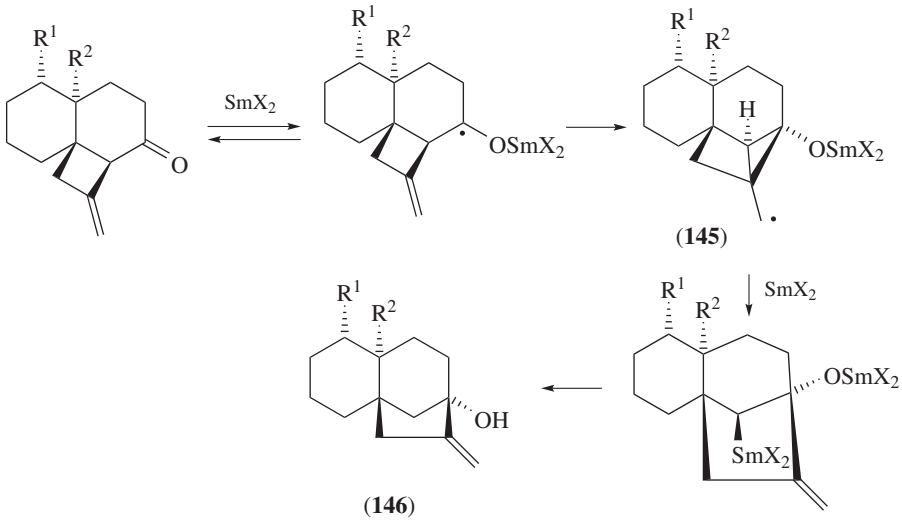

Scheme 64

A diastereoselective reduction reaction is reported in the enantioselective synthesis of (*R*)-(*R*)-(+)-pyrrolsedamine (Scheme 65). The reduction of ketone (**147**) is carried out with $LiAl(OtBu)_3H$, which gave a single *syn* diastereomer. The stereochemical outcome is attributed due to chelation of Li with the carbonyl and the amine functionality. This chelation directs hydride attacks from the least hindered face of the ketone, resulting in the formation of the product.[130] A similar outcome could be explained as a result of a chair-like transition state.[131]

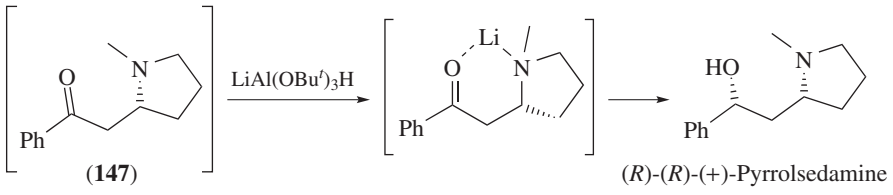

Scheme 65

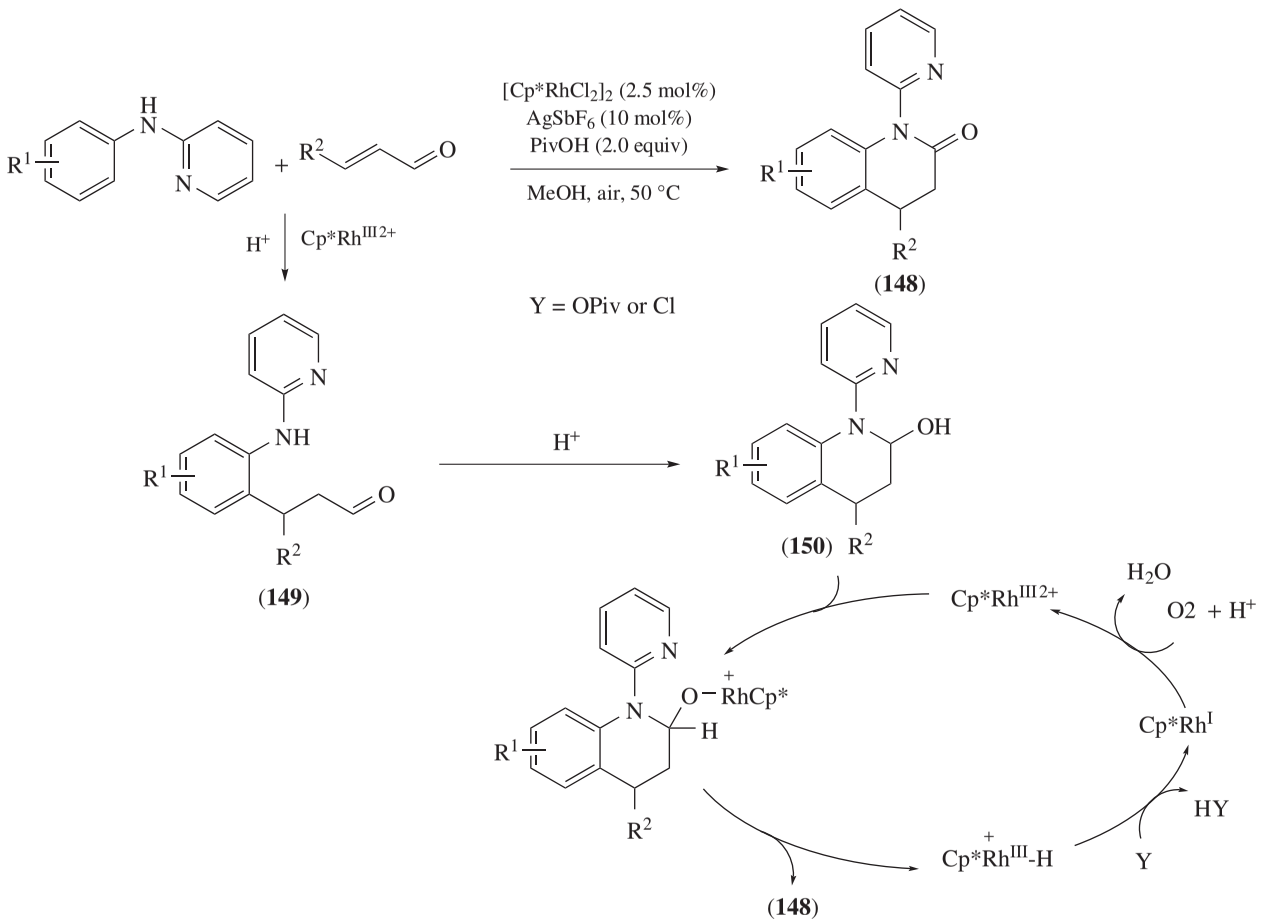
[Cp*RhCl2]2 (2.5 mol%)
AgSbF6 (10 mol%)
PivOH (2.0 equiv)
MeOH, air, 50 °C
H+
Cp*RhIII2+
Y = OPiv or Cl
(148)
(149)
(150)
H+
H2O
O2 + H+
Cp*RhIII2+
Cp*RhI
HY
Y
Cp*RhIII-H
(148)

Scheme 66

Other Reactions

A light-mediated direct chlorination of C(sp^3)–H groups by *N*-chlorosuccinimide occurs in the presence of 5 mol% of arylketones. As the dihalogenated side products are not 1,2-dihalides and 1,1-dihalides, the reaction is suspected to be under kinetic control. As the reaction stops immediately after the light is turned off, the authors suggest that this confirms that the reaction is not a free radical chain reaction.[132] However, it is shown previously that light/dark experiments cannot be used to conclusively rule out a chain mechanism.[133]

The Rh-catalysed coupling of phenylphosphonium salts with α-diazocarbonyl compounds provides 1-naphthols. The reaction is enabled by the initial C–H activation and the subsequent intramolecular Wittig reaction. The H/D exchange experiments suggest the reversibility of the *ortho* C–H activation, while $k_H/k_D = 4.0$ suggests that the C–H activation is likely a turnover step.[134]

An inverse electron-demand Diels–Alder (iEDDA)-type reaction between acetophenone and amidines in the presence of catalytic iodine and base in DMSO provides 1,3,5-trizines. Theoretical and experimental studies suggest that the addition of a primary imine into the secondary imine is the rate-determining step. An *in situ* iodination-based oxidative elimination of formaldehyde, involving DMSO, occurs at a later stage, which ultimately leads to 1,3,5-triazines.[135]

Unsaturated aldehydes convert into saturated esters via a catalytic, enantioselective β-protonation process involving a cooperative activation strategy. Mechanistic studies suggest that NHC carbene acts as the catalyst, while the Brønsted acid activates the aldehyde and provides, in addition to the NHC catalyst, steric interactions near the β-position, enhancing facial selectivity of the protonation step. Base selection determines selects between enolate and homoenolate reactivity, and solvent selection avoids an undesired oxidative pathway.[136] (ee)

A rhodium-catalysed C–H functionalization/cyclization reaction of *N*-arylpyridin-2-amines with α,β-unsaturated aldehydes provides dihydroquinolinone derivatives (**148**) (Scheme 66). Kinetic isotope experiments indicate that C–H cleavage is not involved in the rate-determining step. The active catalyst $Cp^*Rh(III)^{2+}$, generated by $[RhCp^*Cl_2]_2$ and $AbSbF_6$, couples the two starting materials producing (**149**). Under acid catalysis, (**149**) is converted into (**150**). Intermediate (**150**) is converted into (**148**) via a catalytic cycle involving ligand exchange, β-hydride elimination, and the regeneration of $Cp^*Rh(III)^{2+}$ via reductive-elimination and oxidation pathways.[137]

DFT investigations of an NaH-promoted rearrangement of benzaldehyde and 1-cannamoylcyclopropanecarboxamide show a cooperative participation of water, solvent DMSO, and counterion Na^+ in the rate-determining ring-opening cyclization step.[138]

A DABCO-catalysed Cloke–Wilson rearrangement reaction provides ring expansion of cyclopropyl ketones to 2,3-dihydrofurans. Isolation of the zwitterionic intermediate and an experiment with a stereochemical probe suggest that the reaction proceeds via an S_N1-type ring process.[139]

References

1 Chan, C. K., Tsai, Y. L., and Chang, M.-Y., *Org. Lett.*, **19**, 1358 (2017).
2 Mohri, T., Ogura, Y., Towada, R., and Kuwahara, S., *Tetrahedron Lett.*, **58**, 4011 (2017).
3 Niu, Q., Xing, L. L., and Li, C. B., *J. Chem. Res.*, **41**, 358 (2017).
4 Pujol, A. and Whiting, A., *J. Org. Chem.*, **82**, 7265 (2017).
5 Berthet, M., Songis, O., Taillier, C., and Dalla, V., *J. Org. Chem.*, **82**, 9916 (2017).
6 Yadav, J. S., Dhara, S., and Mohapatra, D. K., *Tetrahedron*, **73**, 1358 (2017).
7 Yamazaki, S., Naito, T., Niina, M., and Kakiuchi, K., *J. Org. Chem.*, **82**, 6748 (2017).

8 Duo, T. M., Robinson, K., Greig, I. R., Chen, H. M., Patrick, B. O., and Withers, S. G., *J. Am. Chem. Soc.*, **139**, 15994 (2017).
9 Leng, W. L., Liao, H. Z., Yao, H., Ang, Z. E., Xiang, S. H., and Liu, X. W., *Org. Lett.*, **19**, 416 (2017).
10 Tay, J. H., Arguelles, A. J., DeMars, M. D., Zimmerman, P. M., Sherman, D. H., and Nagorny, P., *J. Am. Chem. Soc.*, **139**, 8570 (2017).
11 van der Vorm, S., Overkleeft, H. S., van der Marel, G. A., and Codee, J. D. C., *J. Org. Chem.*, **82**, 4793 (2017).
12 Hamzehloueian, M., *C.R. Chim.*, **20**, 508 (2017).
13 Rios-Gutiérrez, M., Daru, A., Tejero, T., Domingo, L. R., and Merino, P., *Org. Biomol. Chem.*, **15**, 1618 (2017).
14 Bhaskararao, B., Jindal, G., and Sunoj, R. B., *J. Org. Chem.*, **82**, 13449 (2017).
15 Morrow, S. M., Bissette, A. J., and Fletcher, S. P., *Tetrahedron*, **73**, 5005 (2017).
16 Su, C. Q., Li, Y. Y., Wang, B., Liu, M. J., Wang, H. J., Wang, W. L., and Liu, F. Y., *J. Phys. Chem. A*, **121**, 2588 (2017).
17 Wu, J. C., Lang, M., and Wang, J., *Org. Lett.*, **19**, 5653 (2017).
18 Alexander, J. R. and Cook, M. J., *Org. Lett.*, **19**, 5822 (2017).
19 Schweigert, I. V. and Koh-Fallet, S. E., *J. Phys. Chem. A*, **121**, 1544 (2017).
20 Li, Y. Z., Shan, C. H., Yang, Y.-F., Shi, F. Q., Qi, X. T., Houk, K. N., and Lan, Y., *J. Phys. Chem. A*, **121**, 4496 (2017).
21 Renzi, P., Hioe, J., and Gschwind, R. M., *J. Am. Chem. Soc.*, **139**, 6752 (2017).
22 Gaisina, K. R., Khlebnikov, A. F., and Novikov, M. S., *Org. Biomol. Chem.*, **15**, 4579 (2017).
23 Anderson, J. C., Campbell, I. B., Campos, S., Rundell, C. D., Shannon, J., and Tizzard, G. J., *Org. Lett.*, **19**, 1918 (2017).
24 Efremova, M. M., Kostikov, R. R., Stepakov, A. V., Panikorovsky, T. L., Shcherbakova, V. S., Ivanov, A. V., and Molchanov, A. P., *Tetrahedron*, **73**, 671 (2017).
25 Bagryanskaya, I., Fedin, M., Gorbunov, D., Gritsan, N., Gurskaya, L., Kazantsev, M., Polienko, Y., Stass, D., and Tretyakov, E., *Tetrahedron Lett.*, **58**, 478 (2017).
26 Akaev, A. A., Villemson, E. V., Vorobyeva, N. S., Majouga, A. G., Budynina, E. M., and Melnikov, M. Y., *J. Org. Chem.*, **82**, 5689 (2017).
27 Wang, P., Gao, Y., Zhao, Y., Liu, W., and Wang, Y., *J. Org. Chem.*, **82**, 13109 (2017).
28 Zhang, H.-H. and Yu, S. Y., *J. Org. Chem.*, **82**, 9995 (2017).
29 Das, T. K., Mondal, S., Gonnade, R. G., and Biju, A. T., *Org. Lett.*, **19**, 5597 (2017).
30 Bahamonde, A., Murphy, J. J., Savarese, M., Bremond, E., Cavalli, A., and Melchiorre, P., *J. Am. Chem. Soc.*, **139**, 4559 (2017).
31 Milen, M., Dancso, A., Foldesi, T., and Volk, B., *Tetrahedron*, **73**, 70 (2017).
32 Xiong, J., Wei, X., Yan, Y. M., and Ding, M. W., *Tetrahedron*, **73**, 5720 (2017).
33 Yan, Y. M., Rao, Y., and Ding, M. W., *J. Org. Chem.*, **82**, 2772 (2017).
34 Tuguldurova, V. P., Fateev, A. V., Malkov, V. S., Poleshchuk, O. K., and Vodyankina, O. V., *J. Phys. Chem. A*, **121**, 3136 (2017).
35 Reid, J. P. and Goodman, J. M., *Org. Biomol. Chem.*, **15**, 6943 (2017).
36 Lin, Y. C., Hatzakis, E., McCarthy, S. M., Reichl, K. D., Lai, T. Y., Yennawar, H. P., and Radosevich, A. T., *J. Am. Chem. Soc.*, **139**, 6008 (2017).
37 Tien, C.-H., Adams, M. R., Ferguson, M. J., Johnson, E. R., and Speed, A. W. H., *Org. Lett.*, **19**, 5565 (2017).
38 Wang, G. J., Fu, Z. Q., and Huang, W., *Org. Lett.*, **19**, 3362 (2017).
39 Wang, Y., Liu, H. X., Zhang, X. F., Zhang, Z. L., and Huang, D. G., *Org. Biomol. Chem.*, **15**, 9164 (2017).
40 Albano, S., Olivo, G., Mandolini, L., Massera, C., Ugozzoli, F., and Di Stefano, S., *J. Org. Chem.*, **82**, 3820 (2017).
41 He, W., Zhuang, J. P., Yang, Z. H., and Xu, J. X., *Org. Biomol. Chem.*, **15**, 5541 (2017).
42 Li, H. Y., Luo, J. S., Li, B.-J., Yi, X. Z., and He, Z. J., *Org. Lett.*, **19**, 5637 (2017).
43 Nykaza, T. V., Harrison, T. S., Ghosh, A., Putnik, R. A., and Radosevich, A. T., *J. Am. Chem. Soc.*, **139**, 6839 (2017).
44 Subasi, N. T., Yalcinkaya, H., and Demir, A. S., *Tetrahedron*, **73**, 4329 (2017).
45 Simon, A., Lam, Y. H., and Houk, K. N., *J. Org. Chem.*, **82**, 8186 (2017).
46 Costagliola, A., Venault, L., Deroche, A., Venneulen, J., Duval, F., Blain, G., Vandenborre, J., Fattahi-Vanani, M., and Vigier, N., *J. Phys. Chem. A*, **121**, 5069 (2017).
47 Liu, W. X., Zhang, C., Zhang, H., Zhao, N., Yu, Z.-X., and Xu, J., *J. Am. Chem. Soc.*, **139**, 8678 (2017).
48 Jiao, Y. X., Wu, L.-L., Zhu, H.-M., Qin, J.-K., Pan, C.-X., Mo, D.-L., and Su, G.-F., *J. Org. Chem.*, **82**, 4407 (2017).
49 Jin, X. J., Koizumi, Y., Yamaguchi, K., Nozaki, K., and Mizuno, N., *J. Am. Chem. Soc.*, **139**, 13821 (2017).
50 Ortiz, A., Soumeillant, M., Savage, S. A., Strotman, N. A., Haley, M., Benkovics, T., Nye, J., Xu, Z., Tan, Y., Ayers, S., Gao, Q., and Kiau, S., *J. Org. Chem.*, **82**, 4958 (2017).

51 Patil, M., *Org. Biomol. Chem.*, **15**, 416 (2017).
52 Cvrtila, I., Fanlo-Virgos, H., Schaeffer, G., Santiago, G. M., and Otto, S., *J. Am. Chem. Soc.*, **139**, 12459 (2017).
53 Sun, B. M., Gao, L. J., Shen, S. D., Yu, C. X., Li, T. J., Xiea, Y. W., and Yao, C. S., *Org. Biomol. Chem.*, **15**, 991 (2017).
54 Wang, Y., Wei, D. H., and Tang, M. S., *J. Org. Chem.*, **82**, 13043 (2017).
55 Liu, P., Xu, G. Y., and Sun, J. T., *Org. Lett.*, **19**, 1858 (2017).
56 Jiang, Y., Diagne, A. B., Thomson, R. J., and Schaus, S. E., *J. Am. Chem. Soc.*, **139**, 1998 (2017).
57 Zhang, Z. J., Yi, D., Fu, Q., Liang, W., Chen, S. Y., Yang, L., Du, F. T., Ji, J. X., and Wei, W., *Tetrahedron Lett.*, **58**, 2417 (2017).
58 Hamzik, P. J., Goutierre, A. S., Sakai, T., and Danheiser, R. L., *J. Org. Chem.*, **82**, 12975 (2017).
59 Wilkerson-Hill, S. M., Yu, D., Painter, P. P., Fisher, E. L., Tantillo, D. J., Sarpong, R., and Hein, J. E., *J. Am. Chem. Soc.*, **139**, 10569 (2017).
60 Paraja, M. and Valdes, C., *Org. Lett.*, **19**, 2034 (2017).
61 Choudhary, D., Agrawal, C., Khatri, V., Thakuria, R., and Basak, A. K., *Tetrahedron Lett.*, **58**, 1132 (2017).
62 Schoene, J., Abed, H. B., Christmann, M., and Nazare, M., *Tetrahedron Lett.*, **58**, 1633 (2017).
63 Chogii, I., Das, P., Fell, J. S., Scoto, K. A., Crawford, M. N., Houk, K. N., and Njardarson, J. T., *J. Am. Chem. Soc.*, **139**, 13141 (2017).
64 Garcia-Carrillo, M. A., Guzman, A., and Diaz, E., *Tetrahedron Lett.*, **58**, 1952 (2017).
65 Qiu, D., Wang, S., Meng, H., Tang, S. B., Zhang, Y., and Wang, J. B., *J. Org. Chem.*, **82**, 624 (2017).
66 Yang, M. Y., Zou, J. X., Wang, G. Q., and Li, S. H., *J. Phys. Chem. A*, **121**, 1351 (2017).
67 Usami, K. and Okamoto, A., *Org. Biomol. Chem.*, **15**, 8888 (2017).
68 Zeymer, C., Zschoche, R., and Hilvert, D., *J. Am. Chem. Soc.*, **139**, 12541 (2017).
69 Zhang, Z. R. and Collum, D. B., *J. Org. Chem.*, **82**, 7595 (2017).
70 Poock, C. and Kalesse, M., *Org. Lett.*, **19**, 4536 (2017).
71 Downey, C. W., Lee, A. Y. K., Goodin, J. R., Botelho, C. J., and Stith, W. M., *Tetrahedron Lett.*, **58**, 3496 (2017).
72 Chuang, H. Y. and Isobe, M., *J. Org. Chem.*, **82**, 2045 (2017).
73 Li, M. F., Chu, R., Chen, J. H., Wu, X., Zhao, Y., Liu, S. Y., and Huel, W. H., *Org. Lett.*, **19**, 1290 (2017).
74 Pergomet, J. L., Bracca, A. B. J., and Kaufman, T. S., *Org. Biomol. Chem.*, **15**, 7040 (2017).
75 Vamisetti, G. B., Chowdhury, R., and Ghosh, S. K., *Org. Biomol. Chem.*, **15**, 3869 (2017).
76 Wang, H. B., Lu, G., Sormunen, G. J., Malik, H. A., Liu, P., and Montgomery, J., *J. Am. Chem. Soc.*, **139**, 9317 (2017).
77 Hayashi, M. and Matsubara, R., *Tetrahedron Lett.*, **58**, 1793 (2017).
78 Grayson, M. N., *J. Org. Chem.*, **82**, 4396 (2017).
79 Guo, J. L. and Wong, M. W., *J. Org. Chem.*, **82**, 4362 (2017).
80 Simon, L. and Paton, R. S., *J. Org. Chem.*, **82**, 3855 (2017).
81 Alsharif, Z., Ali, M. A., Alkhattabi, H., Jones, D., Delancey, E., Ravikumar, P. C., and Alam, M. A., *New J. Chem.*, **41**, 14862 (2017).
82 Beltran, F., Fabre, I., Ciofini, I., and Miesch, L., *Org. Lett.*, **19**, 5042 (2017).
83 Li, Z., Li, J. S., and Yang, J. Y., *J. Chem. Res.*, **41**, 168 (2017).
84 Farren-Dai, M., Thompson, J. R., Bernardi, A., Colombo, C., and Bennet, A. J., *J. Org. Chem.*, **82**, 12511 (2017).
85 Li, X.-Y., Han, C. H., Yao, H. Q., and Lin, A. J., *Org. Lett.*, **19**, 778 (2017).
86 Bhattacharjee, D., Sutradhar, D., Chandra, A. K., and Myrboh, B., *Tetrahedron*, **73**, 3497 (2017).
87 Charris-Molina, A., Castillo, J. C., Macias, M., and Portilla, J., *J. Org. Chem.*, **82**, 12674 (2017).
88 Liu, S. S., Shao, N., Li, F. Z., Yang, X. C., and Wang, M. C., *Org. Biomol. Chem.*, **15**, 9465 (2017).
89 Liu, J. L., Zhang, Y. T., Liu, H. F., Zhou, L., and Chen, J., *Org. Lett.*, **19**, 5272 (2017).
90 Merad, J., Maier, T., Rodrigues, C. A. B., and Maulide, N., *Monatsh. Chem.*, **148**, 57 (2017).
91 Schnitzer, T. and Wennemers, H., *J. Am. Chem. Soc.*, **139**, 15356 (2017).
92 von der Heiden, D., Bozkus, S., Klussmann, M., and Breugst, M., *J. Org. Chem.*, **82**, 4037 (2017).
93 Baharfar, R., Asghari, S., Zaheri, F., and Shariati, N., *C.R. Chim.*, **20**, 359 (2017).
94 Abraham, R. and Periakaruppan, P., *Tetrahedron Lett.*, **58**, 3057 (2017).
95 Hayashi, Y., Umekubo, N., and Hirama, T., *Org. Lett.*, **19**, 4155 (2017).
96 Samanta, S. S. and Roche, S. P., *J. Org. Chem.*, **82**, 8514 (2017).
97 Zhang, X. H. and MacMillan, D. W. C., *J. Am. Chem. Soc.*, **139**, 11353 (2017).
98 Huang, W., Liu, H., Xu, Y. J., and Lu, C. D., *J. Org. Chem.*, **82**, 10748 (2017).
99 Aitken, R. A., Boubalouta, Y., Chang, D., Cleghorn, L. P., Gray, I. P., Karodia, N., Reid, E. J., and Slawin, A. M. Z., *Tetrahedron*, **73**, 6275 (2017).

100 Depre, D., Vermeulen, W. A. A., Lang, Y., Dubois, J., Vandevivere, J., Vandermeersch, J., Huang, L., and Robiette, R., *Org. Lett.*, **19**, 1414 (2017).
101 Diaz-Munoz, G., Isidorio, R. G., Miranda, I. L., Dias, G. N. D., and Diaz, M. A. N., *Tetrahedron Lett.*, **58**, 3311 (2017).
102 Pugachev, M. V., Bulatov, T. M., Nguyen, T. T. N., Pavelyev, R. S., Gnezdilov, O. I., Lodochnikova, O. A., Islamov, D. R., Kataeva, O. N., Balakin, K. V., and Shtyrlin, Y. G., *Tetrahedron Lett.*, **58**, 766 (2017).
103 Schmidt, R., Ostermeier, M., and Schobert, R., *J. Org. Chem.*, **82**, 9126 (2017).
104 Liu, Y.-F., Ji, P. Y., Xu, J.-W., Hu, Y. Q., Liu, Q., Luo, W.-P., and Guo, C.-C., *J. Org. Chem.*, **82**, 7159 (2017).
105 Triana, V. and Derda, R., *Org. Biomol. Chem.*, **15**, 7869 (2017).
106 Wang, T. D., Kohrt, S., Daniliuc, C. G., Kehr, G., and Erker, G., *Org. Biomol. Chem.*, **15**, 6223 (2017).
107 Nicolaou, K. C., Rhoades, D., Wang, Y. P., Bai, R. L., Hamel, E., Aujay, M., Sandoval, J., and Gavrilyuk, J., *J. Am. Chem. Soc.*, **139**, 7318 (2017).
108 Li, X.-Y., Yuan, W. Q., Tang, S., Huang, Y. W., Xue, J. H., Fu, L. N., and Guo, Q. X., *Org. Lett.*, **19**, 1120 (2017).
109 Kalla, R. M. N., Zhang, Y., and Kim, I., *New J. Chem.*, **41**, 5373 (2017).
110 Peng, C., Zhai, J. J., Xue, M. Q., and Xu, F., *Org. Biomol. Chem.*, **15**, 3968 (2017).
111 Wang, Y., Xing, F., Gu, C.-Z., Li, W.-J., He, L., Dai, B., and Du, G.-F., *Tetrahedron*, **73**, 4501 (2017).
112 Yue, Y. X., Peng, J. S., Wang, D. Q., Bian, Y. Y., Sun, P., and Chen, C. X., *J. Org. Chem.*, **82**, 5481 (2017).
113 Wang, G. Q., Cao, J., Gao, L. Z., Chen, W. X., Huang, W. H., Cheng, X., and Li, S. H., *J. Am. Chem. Soc.*, **139**, 3904 (2017).
114 Debrouwer, W., Hertsen, D., Heugebaert, T. S. A., Boydas, E. B., Van Speybroeck, V., Catak, S., and Stevens, C. V., *J. Org. Chem.*, **82**, 188 (2017).
115 Sun, K., Lv, Y. H., Chen, Y., Zhou, T. T., Xing, Y. Y., and Wang, X., *Org. Biomol. Chem.*, **15**, 4464 (2017).
116 Gaber, H. M., Muhammad, Z. A., Gomha, S. M., Farghaly, T. A., and Bagley, M. C., *Curr. Org. Chem.*, **21**, 2168 (2017).
117 Saheb, V., Hashemi, S. R., and Hosseini, S. M. A., *J. Phys. Chem. A*, **121**, 6887 (2017).
118 Ma, X. Y., Ao, J., Chen, Z. J., and Liu, Y., *J. Chem. Res.*, **41**, 465 (2017).
119 Ding, K., Xu, S., Alotaibi, R., Paudel, K., Reinheimer, E. W., and Weatherly, J., *J. Org. Chem.*, **82**, 4924 (2017).
120 Lee, P. Y., Liang, P. W., and Yu, W. Y., *Org. Lett.*, **19**, 2082 (2017).
121 Morioka, T., Nishizawa, A., Furukawa, T., Tobisu, M., and Chatani, N., *J. Am. Chem. Soc.*, **139**, 1416 (2017).
122 Wang, D. H., Zhang, L., and Luo, S. Z., *Org. Lett.*, **19**, 4924 (2017).
123 Bortolini, O., Chiappe, C., Fogagnolo, M., Massi, A., and Pomelli, C. S., *J. Org. Chem.*, **82**, 302 (2017).
124 Zheng, C. G., Liu, X., and Ma, C., *J. Org. Chem.*, **82**, 6940 (2017).
125 Liu, H. Z., Wang, Z. J., Zhang, H. X., Li, L., Li, N., Wu, M. H., Chen, J. Z., and Zhu, Z. P., *New J. Chem.*, **41**, 4750 (2017).
126 Sun, C.-H., Zeng, Y. L., Xu, B. E., and Meng, L. P., *New J. Chem.*, **41**, 7714 (2017).
127 Tao, C. Z., Wang, B., Sun, L., Yi, J. Y., Shi, D. H., Wang, J., and Liu, W. W., *J. Chem. Res.*, **41**, 25 (2017).
128 Esfandiarfard, K., Mai, J., and Ott, S., *J. Am. Chem. Soc.*, **139**, 2940 (2017).
129 Takatori, K., Ota, S., Tendo, K., Matsunaga, K., Nagasawa, K., Watanabe, S., Kishida, A., Kogen, H., and Nagaoka, H., *Org. Lett.*, **19**, 3763 (2017).
130 Bhosale, V. A., Markad, S. B., and Waghmode, S. B., *Tetrahedron*, **73**, 5344 (2017).
131 Reetz, M. T. and Jung, A., *J. Am. Chem. Soc.*, **105**, 4833 (1983).
132 Han, L., Xia, J.-B., You, L., and Chen, C., *Tetrahedron*, **73**, 3696 (2017).
133 Cismesia, M. A. and Yoon, T. P., *Chem. Sci.*, **6**, 5426 (2015).
134 Li, Y. Y., Wang, Q. A., Yang, X. F., Xie, F., and Li, X. W., *Org. Lett.*, **19**, 3410 (2017).
135 Tiwari, A. R., Nath, S. R., Joshi, K. A., and Bhanage, B. M., *J. Org. Chem.*, **82**, 13239 (2017).
136 Wang, M. H., Barsoum, D., Schwamb, C. B., Cohen, D. T., Goess, B. C., Riedrich, M., Chan, A., Maki, B. E., Mishra, R. K., and Scheidt, K. A., *J. Org. Chem.*, **82**, 4689 (2017).
137 Wu, Z.-J., Huang, K. L., and Huang, Z.-Z., *Org. Biomol. Chem.*, **15**, 4978 (2017).
138 Zhu, L. H., Yuan, H. Y., and Zhang, J. P., *Org. Biomol. Chem.*, **15**, 9127 (2017).
139 Zhang, J. F., Tang, Y. H., Wei, W., Wu, Y., Li, Y., Zhang, J. J., Zheng, Y. S., and Xu, S. L., *Org. Lett.*, **19**, 3043 (2017).